TORSIONAL RESPONSE OF SEISMIC ISOLATED BUILDINGS CONSIDERING ACTUAL DISTRIBUTION OF DESIGN COEFFICIENT OF FRICTION AMONG CURVED SURFACE SLIDERS

A THESIS SUBMITTED TO
THE GRADUATE SCHOOL OF NATURAL AND APPLIED SCIENCES
OF
MIDDLE EAST TECHNICAL UNIVERSITY

BY

UĞUR SERGEN YAŞAR

IN PARTIAL FULFILLMENT OF THE REQUIREMENTS
FOR
THE DEGREE OF MASTER OF SCIENCE
IN
ENGINEERING SCIENCES

SEPTEMBER 2021

Approval of the thesis:

TORSIONAL RESPONSE OF SEISMIC ISOLATED BUILDINGS CONSIDERING ACTUAL DISTRIBUTION OF DESIGN COEFFICIENT OF FRICTION AMONG CURVED SURFACE SLIDERS

submitted by **UĞUR SERGEN YAŞAR** in partial fulfillment of the requirements for the degree of **Master of Science** i**n Engineering Sciences, Middle East Technical University** by,

Prof. Dr. Halil Kalıpçılar
Dean, Graduate School of **Natural and Applied Sciences** _____

Prof. Dr. Murat Dicleli
Head of the Department, **Engineering Sciences** _____

Prof. Dr. Murat Dicleli
Supervisor, **Engineering Sciences, METU** _____

Examining Committee Members:

Assoc. Prof. Dr. Ferhat Akgül
Engineering Sciences, METU _____

Prof. Dr. Murat Dicleli
Engineering Sciences, METU _____

Prof. Dr. Ahmet Hakan Argeşo
Manufacturing Engineering, Atılım University _____

Date: 03.09.2021

I hereby declare that all information in this document has been obtained and presented in accordance with academic rules and ethical conduct. I also declare that, as required by these rules and conduct, I have fully cited and referenced all material and results that are not original to this work.

Name Last name : Uğur Sergen Yaşar

Signature :

ABSTRACT

TORSIONAL RESPONSE OF SEISMIC ISOLATED BUILDINGS CONSIDERING ACTUAL DISTRIBUTION OF DESIGN COEFFICIENT OF FRICTION AMONG CURVED SURFACE SLIDERS

Yaşar, Uğur Sergen
Master of Science, Engineering Sciences
Supervisor : Prof. Dr. Murat Dicleli

September 2021, 100 pages

In this study, torsional response of seismic isolated buildings with curved surface slider (CSS) isolators are investigated considering actual distribution of design coefficient of friction in the CSS isolator. For this purpose, experimental results are used to characterize frictional properties of CSS isolator. Then, nonlinear response history analyses are performed using three-dimensional model of 3 structures that are developed based on a hospital structure. Torsional response of the structures and the parameters that influence the torsion are investigated.

The analyses revealed that if the effect of contact pressure and heating on the friction coefficient is not taken into account, the additional displacements in the CSS isolators due to torsion are significantly underestimated. It is also found that increasing the number of groups within isolation system is an effective way to reduce torsion, if the isolators are seperated into groups based on axial loads on them.

Keywords: Seismic Base Isolation, Curved Surface Slider, Friction Coefficient, Torsional Response

ÖZ

DEPREM YALITIMLI BİNALARDA EĞRİ YÜZEYLİ KAYICI YALITIM BİRİMLERİNDEKİ TASARIM SÜRTÜNME KATSAYISININ GERÇEK DAĞILIMI DİKKATE ALINARAK YAPININ BURULMA DAVRANIŞININ İNCELENMESİ

Yaşar, Uğur Sergen
Yüksek Lisans, Mühendislik Bilimleri
Tez Yöneticisi: Prof. Dr. Murat Dicleli

Eylül 2021, 100 sayfa

Bu çalışmada eğri yüzeyli kayıcı (EYK) yalıtım birimleri kullanılarak deprem yalıtımı uygulanan yapılardaki burulma davranışı yalıtım birimlerindeki sürtünme katsayısının gerçek dağılımı dikkate alınarak incelenmiştir. Bu amaçla, sürtünme katsayısını etkileyen faktörler tespit edilmiştir. Daha sonra, bir hastane yapısı temel alınarak oluşturulan deprem yalıtımlı 3 adet yapının üç boyutlu sayısal modelleri oluşturularak, zaman tanım alanında doğrusal olmayan analizler yapılmış ve yapılardaki burulma davranışını etkileyen faktörler incelenmiştir.

Analizler sonucunda, EYK yalıtım birimlerinin sayısal modellerinde, sürtünme katsayısını etkileyen basınç ve ısınma etkilerinin dikkate alınmadığı takdirde, yalıtım birimlerinde oluşacak burulma kaynaklı ilave yer değiştirmelerin tespit edilemeyeceği görülmüştür. Yalıtım birimleri eksenel yüklerine göre gruplandırıldığında, grup sayısının burulma davranışını azaltmada etkili olduğu gözlemlenmiştir.

Anahtar Kelimeler: Deprem Yalıtımlı Yapıda Burulma, Eğri Yüzeyli Sürtünmeli İzolatör, Sürtünme Katsayısı

ACKNOWLEDGMENTS

I would like to express my gratitude to my supervisor, Prof. Dr. Murat Dicleli, for his trust, patience, and support throughout my studies.

I thank my friend Talha Orhan for his genuine interest and suggestions on various technical subjects.

My thanks go to a great person and engineer, Muhsin Demir, for his trust, and guidance from the first day we met.

I thank my dear friends, Burak Terzioğlu and Mustafa Berat Özer, who have eased this process for me with their support and invaluable friendship.

I sincerely thank my sister for her trust and support since my childhood. Finally, I thank my parents, to whom I am indepted for their endless support and understanding they have shown throughout my life.

TABLE OF CONTENTS

LIST OF TABLES

TABLES

LIST OF FIGURES

FIGURES

CHAPTER 1

INTRODUCTION

Base isolation is a type of passive structural control application; efficient and widely accepted method to mitigate earthquake-induced forces in structures (e.g. buildings, bridges). The base isolation is also becoming an economic solution regarding the performance criteria of structures. A conventional structure would require to perform within its elastic limit to achieve the immediate occupancy performance level that imposed for base isolated structures in codes (Erdik 2020), which would lead uneconomical solution when compared to isolated counterpart of the structure.

The main principle of base isolation is to decouple the structure from dynamic event by interposing structural elements, namely isolator or bearing, between the stucture and foundation (Kelly, 1997). In order to reduce lateral forces on structure induced by seismic motion, the vibration periods of the structure are shifted by means of isolation layer installed between superstructure and foundation. Meanwhile, the isolation system dissipates most of the earthquake-induced energy by cyclic behavior and protects the other structural elements. The effect of the isolation system on reducing seismic forces might be best understood by theory of dynamics of structures and explained as follows. In simplified seismic analysis, a structure can be treated as single degree of freedom system (SDOF) having first natural period T and damping ratio ζ. The base shear,V_b, expected in structure due to earthquake-induced forces can be expressed as a function of the structure's mass m, first natural period T and damping ratio ζ, as follows:

$$V_b = m \cdot A(T, \zeta) \tag{1-1}$$

where $A(T, \zeta)$, in units g, corresponding spectral acceleration value for T and ζ. As shown in Figure 1-1 for typical elastic design spectrum, the spectral acceleration decreases as the natural period of the structure increases, thus, the earthquake-induced forces in the structure are reduced (Chopra, 2012).

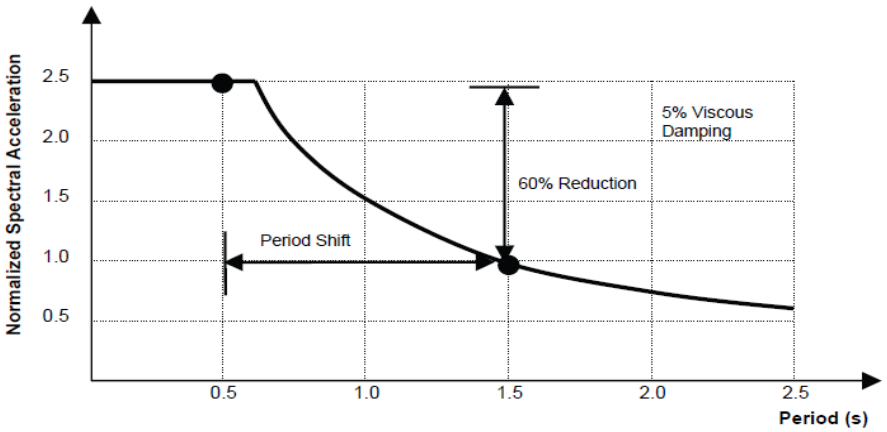

Figure 1-1: Typical period-spectral acceleration relationship (Buckle et al., 2006).

The Curved Surface Slider (CSS) is a sliding type isolator consists of a slider and spherical concave plate on which the slider moves freely. The spherical concave surface provides recentering force as the slider rise along the surface while the friction between the slider and surface provides energy dissipation. The CSS isolator typically made of stainless steel alloy (e.g. austenitic stainless steel) and the side of the slider in contact with sliding surface is coated with low-friction composite material (e.g. PTFE). The Friction Pendulum Bearing (FPB) is the North American counterpart of the CSS isolator, and first proposed by Zayas et al. (1987).

The Double Curved Surface Slider (DCSS or double CSS) isolator, is a special type of CSS isolator that consist of two concave sliding surface seperated by either articulated or rigid slider.The double CSS isolator has some adventageous over the single CSS. Having two sliding surface doubles the displacement capacity of the DCSS compared to the single CSS, and decreases the frictional heating by reducing the sliding velocity (McVitty and Constantinou, 2015). The double CSS exhibits

the same bilinear force-displacement behavior in horizontal direction as that of single CSS. Thus, the mathematical model developed for single CSS isolator can be used for double CSS with minor modifications.

1.1 Problem definition

The torsional response in base isolated structures results from (1) eccentricity in isolation system, (2) eccentricities above the isolation level (superstructure eccentricity), (3) torsional and rocking ground motions (Wolff et al., 2014). The eccentricity in isolation system is defined as the distance from the center of mass (CM) to the center of rigidity (CR) of the isolation system. Building codes encourages to design an isolation system so that the eccentricity between CM and CR are minimized. The torsional response of CSS-based isolation system is expected to be small (Wolff et al., 2014), as the CR coincides with CM of the isolation system by constantly shifting during an seismic event, and thus compensates the eccentricity (Almazan and de la Llera, 2003) owing to fact the lateral resisting force in a CSS isolator is function of the supported weight. Moreover, the lateral resisting force is linearly proportional to the supported weight if all CSS isolators within the system have same geometry and friction properties and are subjected to the same displacement. (Skinner et al., 2011). That is, if the geometric and friction properties are identical for all isolators during the motion and, they undergo same displacement, then, the total lateral resisting force can be expressed as a constant times the total supported weight, which in turn, indicates that the CR coincides with CM of the isolation system. However, this is extremely unlikely for the reasons described in the following. First, lateral resisting force in a CSS isolator depends on the effective radius of curvature, instantenous axial load, friction coefficient and the relative displacement, as shown in Figure 1-2. These properties except the radius of curvature can deviate significantly among isolators during the course of a seismic motion.

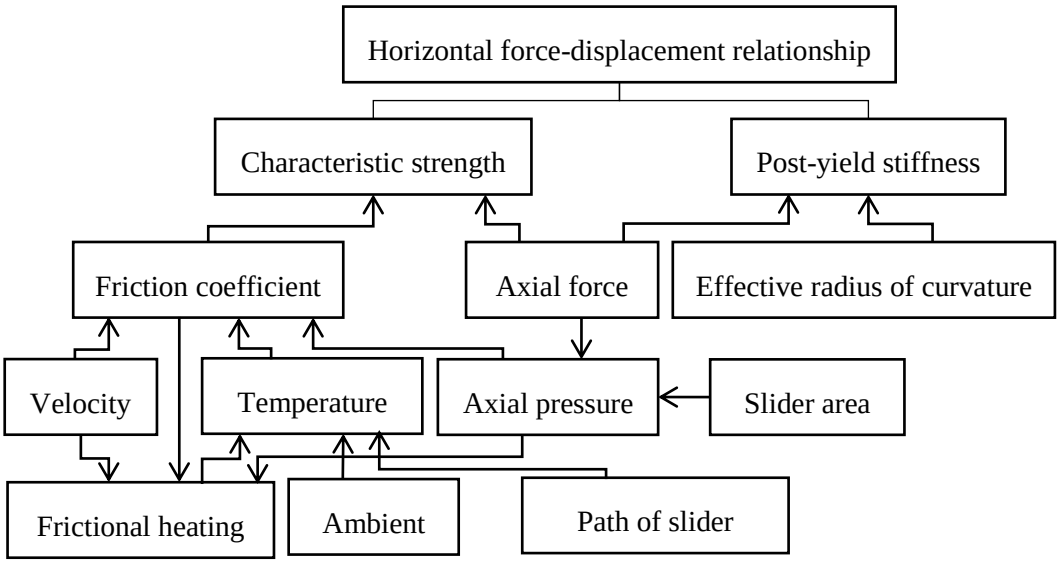

Figure 1-2. Interdependence of parameters that define the horizontal force-displacement behavior of an CSS isolator (adapted from Kumar et al., 2015).

Nonlinear Response History Analysis (NLRHA) is performed to predict the nonlinear behavior of the isolators and response of the entire isolation system. The latter is especially important for the following reasons. First, isolators are sized and manufactured according to the project-specific displacement demand. Second, additional displacements due to torsion may occur at corner isolators, which may cause excessive displacements (Dicleli, 2020). The NLRHA requires a mathematical model that governs the lateral force-displacement behavior of the CSS isolators. There are number of studies dedicated to develop mathematical models to define the behavior of the single and double CSS isolators under dynamic conditions (Fenz and Constantinou, 2008a; Kumar, 2015; Bao and Becker, 2019). These models have been incorporated in corresponding elements of commercial structural analysis programs such as Sap2000 and ETABS (Computers and Structures, 2016). Furthermore, an open source structural analysis program OpenSees (McKenna et al., 2010) has special elements for the CSS isolators. The numerical models of the CSS isolators in aforementioned programs have achieved great deal of accuracy in predicting the response of these isolators, as they have

been validated by experimental studies over the years (Scheller and Constantinou, 1999; Mosqueda et al., 2004; Fenz and Constantinou, 2008a; Kumar et al., 2014).

Behavior of a CSS isolator greatly depends on the friction coefficient at sliding interface, which vary once sliding commence in a seismic event. Experimental studies have showed that the coefficient of friction in the CSS isolators depends on number of factors, most influentual being, the sliding velocity, the contact pressure and the temperature at sliding interface (Constantinou et al., 2007). The main reason for the change in temperature at sliding interface is the heating due to friction between the slider and sliding surface that occurs during cyclic motion. The displacement response is significantly underestimated if the effect of frictional heating is not accounted for (Kumar et al., 2014). Although the influence of these factors on response are accounted by many studies, and the effect of velocity has been incorporated, some analysis programs lack of capability to account for the pressure and heating effects in friction model of the CSS isolator. Thus, the variations in friction coefficient are disregarded by such programs, leading unconservative results.

The CSS isolators are subjected to compressive axial (vertical) loads primarly because of static loads on them. The friction coefficient varies with contact pressure that results from axial load on isolator which may vary significantly during a seismic event due to overturning moments and vertical component of ground accelerations, of which the former especially is pronounced in slender structures (Almazan and de la Llera 2003). Furthermore, the distribution of static axial loads on isolators depends on the project-specific mass distribution of the structure. Thus, an isolation system may work under a wide range of axial loads. This might be especially true for large applications where the isolation system supports two or more superstructures, a situation that shows up in a hospital complex, or it can be observed in structures that have setbacks in elevation. Even for a system where isolators have identical geometric properties, the friction coefficient can differ among the isolators significantly since the contact pressures can differ due to aforementioned reasons. This may cause uneven displacements

among isolators. To alleviate this problem, theoretically, isolator dimensions can be altered such that a target friction coefficient is achieved for each isolator in the system. However, this requires each isolator have manufactured seperately which leads to an uneconomic solution (Mazza 2017). In practice of large structures, isolators can be divided into groups in accordance with axial loads to reduce the plan size of the isolators (Higashino and Okamoto 2006). The isolators with similar axial loads are grouped together. Another reason to group isolators is to design an isolator size for each group, seperately, so that the friction coefficient in isolators within respective group is close to each other, and also close to a target friction coefficient (Dicleli, 2020). Therefore, friction properties of the isolators are not deviate from a target value while manufacturing costs are taken into account. However, variation of friction coefficient among individual isolators in a group may still occurs as the axial loads vary. This will induce eccentricity even if the average friction coefficient of a group is equal to the target friction coefficient.

1.2 Past studies

Torsional response of the isolated structures still an open area of research. Nagarajaiah et al. (1993) was among the first to conduct a study on torsional response in sliding-based isolation system. The main objective was to identify the key parameters associated with both isolation system and superstructure, that lead to torsion in structure. The important conclusions of that study were (1) the main source of torsion in isolated structures is due to eccentricity in superstructure, (2) the torsional amplification at corner isolators increases as the ratio of first translational period to first torsional period of the isolated structure increases. Although, the isolation system was friction based, only the effect of sliding velocity on the friction coefficient was considered, pressure and heating efffects were not mentioned.

Almazan and de la Llera (2003) were among the first to observe the torsion in structures isolated with CSS isolators due to variations in properties of the CSS

isolators. In that study, although the friction coefficient was considered to be constant (i.e. Coulomb friction model) for all isolators, the significant variations in axial loads on the isolators due to overturning moments were mentioned as the main reason for the torsional amplifications in structures.

Wolff et al. (2014) introduced an equation for the torsional amplification factor for corner isolators, based on experimental results. The main conclusions drawn from that study were (1) eccentricities in superstructure increases the torsional amplifications, though, the extent of increase is dependent on the ground motions used, (2) the torsional amplifications in CSS-based isolation system ranges between 1.0 and 1.1 even for relatively large eccentricities.

Mazza (2017) conducted a study on a base isolated structure with CSS isolators to examine the torsional response considering the near-fault effects of ground motions. The velocity and axial load depending friction coefficient was considered. One of the main conclusions of the study was that the torsional response in structure isolated with CSS isolators could be significant, especially for near-fault sites, controverting previous studies for which torsional response is negligible in sliding-based systems. The study also investigated an optimized isolation system layout that minimize the eccentricity in the system while posing an economical solution.

1.3. Research objective

The key objectives of this study are (1) understand the importance of the friction model on response of the CSS isolators, and on the torsional response of the isolation system, (2) identify the parameters that influence the torsion on the isolation system, (3) develop and compare the methods that can be used to calculate slider contact area for the CSS isolators to minimize torsion on the isolation system.

CHAPTER 2

MODELING CURVED SURFACE SLIDER ISOLATOR

The basic principle of operation of a CSS isolator when the slider in motion is shown in Figure 2-1. The force required to impose displacement on the slider is combination of restoring force and friction force which explained briefly as follows. As the slider moves along the sliding surface, the supported mass rises vertically due to concave spherical geometry of the surface. This produce recentering force back to initial position of the slider (pendulum motion). Moreover, the friction force acts opposite to the direction of the movement due to friction between the slider and sliding surface.

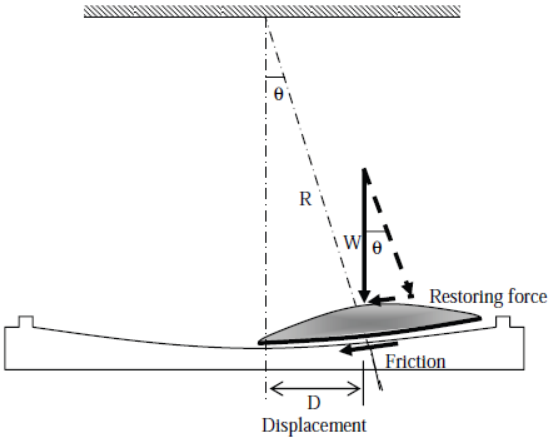

Figure 2-1. Operation of an CSS isolator (Force vectors shown for sliding to the right) (Buckle et al., 2006).

From equilibrium in the vertical and horizontal directions, the horizontal force-displacement relationship for the CSS isolator can be expressed as follows (Soong and Constantinou, 1994):

$$F_h = \frac{N}{R_{eff} \cdot \cos\theta} u + \frac{F_f}{\cos\theta} \tag{2-1}$$

where F_h is the total resisting horizontal force in the isolator, u is the horizontal displacement, θ is the angle between normal of the isolator and vertical axis, N is the instantenous compressive axial (vertical) force on the isolator, R radius of the spherical concave surface, R_{eff} is the effective radius of the concave surface, which defined as the radial distance from the center of spherical surface to the pivot point of the slider, F_f is the friction force acting on the isolator. The instanteneous axial force on the isolator, N, can be synthesized by

$$N = W\left(1 + \frac{\ddot{u}_{gv}}{g} + \frac{N_{om}}{W}\right) \tag{2-2}$$

where W is the supported weight, $\ddot{u}_{gv}$ is the vertical component of the ground acceleration, N_{om} is the additional axial force due to overturning moments.

For most applications, θ is small ($\theta < 0.3R_{eff}$), approximating $\cos\theta \approx 1$ the lateral force-displacement can be expressed as follows:

$$F_h = \frac{N}{R_{eff}} u + F_f \tag{2-3}$$

where all terms previously defined. The friction force acting on the slider can be expressed as follows:

$$F_f = \mu N \tag{2-4}$$

Substituting equation (2-4) into (2-3) the following can be obtained:

$$F_h = \frac{N}{R_{eff}} u + \mu N \mathrm{sgn}(\dot{u}) \tag{2-5}$$

where μ is the coefficient of friction, $\dot{u}$ is the velocity of the slider relative to the sliding surface and sgn() is the sign function to represent direction of movement and other terms were defined previously.

The equation of motion for an individual CSS isolator subjected to an external force is formulated as follows:

$$m\ddot{u}(t) + c\dot{u}(t) + F_h u(t) = P(t) \quad (2\text{-}6)$$

where m is the mass, c is damping coefficient, F_h is the horizontal resisting force in the isolator and $u(t)$, $\dot{u}(t)$, $\ddot{u}(t)$ are the displacement, velocity and acceleration of the isolator relative to its fixed base at time t, and P(t) is the external force. The equation of motion applies during the course of sliding. However, when the slider stops, the following differential equation holds:

$$\dot{u} = 0 \quad (2\text{-}7)$$

Equation (2-5) can be used to model and analyze if there is one CSS isolator in the system because of the following reasons. For large isolation systems, the isolators may undergo different displacements during the course of motion. Thus, multiple stick-slip conditions that regulates transition from static to kinetic phase of an CSS isolator are required for each step in analysis (Su et al., 1987), which might be time consuming as the number of isolators increases. Furthermore, the differential equation that governs the static phase of the isolators is expressed by equation (2-7) whereas equation (2-6) applies for kinetic phase. Hence, solution of two different model is required to define behavior of the CSS isolators. Finally, numerical solution of a differential equation that have discontinuities such as equation (2-6) suffers from the following effect. According to Feldstein and Goodman (1973) if any algorithm of order $m > 1$ is applied to a differential equation with discountinuties, its order of convergence collapses to m=1 after only one discontinuity (Constantinou et al., 1990). For the reasons described above, equation (2-5) is seldom used for analysis of multiple CSS isolators. Instead, to date, two models, Bouc-Wen and Rate-independent plasticity models have been implemented in analysis programs such as 3D-BASIS, Sap2000, ETABS and OpenSees. These models are described in the next.

2.1 Multi-linear plasticity model

This model can be used to characterize bi-linear force-displacement behavior of a CSS isolator, using a set of points on force-displacement hysteresis obtanied from experiments. However, typically, internal deformations within shear degrees of freedom are assumed to be independent from each another, which decrease the accuracy of the model (Mosqeuda et al., 2004). Moreover, variations in friction coefficient cannot be captured.

2.2 Bouc-Wen model

Bouc-Wen model is based on Park et al. (1986) and proposed by Nagarajaiah et al. (1991) for sliding type isolators including the CSS isolator. The sign function in equation (2-6) is replaced by hysteretic variable, resulting in the following expression for uniaxial behavior:

$$F_h = \frac{N}{R_{eff}} u + \mu N Z \tag{2-8}$$

and

$$\frac{dZ}{dt} = \frac{1}{D_{yield}} [A - |Z|^{\eta}(sgn(\dot{u}Z)\gamma + \beta)]\dot{u} \tag{2-9}$$

where N is the instanteneous axial force on the isolator, R_{eff} is the effective radius of curvature, u is the relative displacement, μ is the coefficient of friction, Z is the hysteretic variable governed by equation (2-9), t is the time, D_{yield} is the yield displacement of the isolator, $\dot{u}$, is the sliding velocity, A, η, γ, β are the dimensionless variables that control the shape of the force-displacement hysteresis.

For bi-directional model, the constitutive equations that regulates force-displacement behavior in two horizontal orthogonal directions are expressed as follows:

$$F_x = \frac{N}{R_{eff}} u_x + \mu N Z_x \tag{2-10}$$

$$F_y = \frac{N}{R_{eff}} u_y + \mu N Z_y \tag{2-11}$$

where F_x, F_y are the horizontal resisting forces in principal x, y directions, in CSS isolator, u_x, u_y are the displacements, Z_x, Z_y are the hysteretic terms governed by differential equations (2-12) and (2-13). The coupling terms introduced to these equations provide an accurate simulation of coupling of the friction response in shear degrees of freedoms.

$$\dot{Z}_x = \frac{1}{Y}\left(A\dot{u}_x - Z_x^2(\mathrm{sgn}(\dot{u}_x Z_x)\gamma + \beta) + Z_x Z_y\left(\mathrm{sgn}\left(\dot{u}_y Z_y\right)\gamma + \beta\right)\right) \tag{2-12}$$

$$\dot{Z}_y = \frac{1}{Y}\left(A\dot{u}_y - Z_y^2\left(\mathrm{sgn}\left(\dot{u}_y Z_y\right)\gamma + \beta\right) + Z_x Z_y(\mathrm{sgn}(\dot{u}_x Z_x)\gamma + \beta)\right) \tag{2-13}$$

where $\dot{Z}_x, \dot{Z}_y$ are the first derivative of the hysteretic terms,$\dot{u}_x$, $\dot{u}_y$ are the sliding velocities in principal x, y directions, and other terms are already defined.

The Bouc-Wen model is used within the predefined nonlinear elements in the Sap2000, ETABS and 3D-BASIS suite of programs for governing model of the CSS isolator. According to (CSI, 2016) and (Fenz and Constantinou, 2008) the values for $A = 1$, $\gamma = \beta = 0.5$ and $\eta = 2$ are used in these programs.

2.3 Rate-independent plasticity model

The detailed description of this model can be found in other studies (Mosqueda et al., 2004; Huang, 2002; Gandelli, 2017). For bi-directional model of the CSS isolator, the resisting force can be expressed as follows:

$$\mathbf{F} = K_2\mathbf{U} + \mathbf{F}_p \tag{2-14}$$

where **F** is the vector of resisting force, **U** is the vector of displacement, K_2 is the post-yield (sliding) stiffness, $\mathbf{F}_p$ is the vector of hysteretic force. The hysteretic term is modeled as elastic-perfectly plastic with initial stiffness, $K_1 - K_2$ and yield force Q_D using following equations:

$$\mathbf{F}_{\mathrm{p}} = (\mathrm{K}_1 - \mathrm{K}_2)(\mathbf{U} - \mathbf{U}_{\mathrm{p}}) \tag{2-15}$$

where $\mathbf{U}_{\mathrm{p}}$ is the vector of plastic displacement. For bi-directional motion, the CSS isolators exhibit istropic behavior and a circular yield condition is proposed. The yield surface satisfies the condition

$$\boldsymbol{\phi}(\mathbf{F}_{\mathrm{p}}) = |\mathbf{F}_{\mathrm{p}}| - \mathrm{Q}_{\mathrm{D}} \leq 0 \tag{2-16}$$

where the change in plasitc deformation, $\dot{\mathbf{U}}_p$, is zero for $\boldsymbol{\phi}(\mathbf{F}_{\mathrm{p}}) < 0$. For $\boldsymbol{\phi}(\mathbf{F}_{\mathrm{p}}) = 0$, an associate plastic flow rule with slip rate $\gamma \geq 0$ is assumed as follows:

$$\dot{\mathbf{U}}_{\mathrm{p}} = \gamma \frac{\partial \boldsymbol{\phi}(\mathbf{F}_{\mathrm{p}})}{\partial \mathbf{F}_{\mathrm{p}}} = \gamma \frac{\mathbf{F}_{\mathrm{p}}}{|\mathbf{F}_{\mathrm{p}}|} \tag{2-17}$$

The loading/unloading conditions are described by the Kuhn-Tucker complimentary conditions

$$\gamma \geq 0, \qquad \boldsymbol{\phi}(\mathbf{F}_{\mathrm{p}}) \leq 0, \qquad \gamma\boldsymbol{\phi}(\mathbf{F}_{\mathrm{p}}) = 0 \tag{2-18}$$

and the consistency requirement

$$\gamma\dot{\boldsymbol{\phi}}(\mathbf{F}_{\mathrm{p}}) = 0 \tag{2-19}$$

The equations (2-14) to (2-19) are utilized to compute resisting force **F** by using the return-mapping algorithm for plasticity (Simo and Hughes, 1998).

The rate-independent plasticity model is used within two elements, which are available in OpenSees library, namely, 'singleFPBearing' and 'FPBearingPTV'. The latter is used in this study along with OpenSees to model and analyze the CSS isolators.

The difference between Bouc-Wen and Rate-independent plasticity model is negligible for large values of initial stiffness of the CSS isolator according to an analytical study of Huang (2002). The Bouc-Wen model with parameters $\mathrm{A} = 1$ and $\gamma + \beta = 1$, is smoothed form of Rate-independent plasticity model under conditions that typically occurs in seismic applications. For displacements much larger than yield displacement$(\mathrm{u} \gg \mathrm{D}_{\mathrm{yield}})$, the response of the two models are similar but a smooth transition from elastic to plastic states shows up in response

with Bouc-Wen model. This certainly applies for the CSS isolators in which the yield displacements are on the order of 0.1-2 mm which at least one or two order of magnitude smaller than typical displacements. Huang (2002) also found that both models will likely give acceptable results in most instances, however, computational effort is needed to solve highly nonlinear differential equation (2-9) of Bouc-Wen model. Indeed, a number of studies addressed the issue associated with the solution for hysteretic variable, Z. Nagarajaiah et al. (1989) developed a special solution algorithm that utilize semi-implicit Runge-Kutta method for the solution of systems with Bouc-Wen model. Fenz et al. (2008b) showed a Matlab routine with 'stiff' differential equation solver for solution of equation (2-9). In those studies, state-space representation of the equation of motion of isolation system and superstructure is needed to solve for hysteretic variable, which requires to convert second order differential equations to a set first order. In a similar study, Ulker-Kaustell (2017) used Bouc-Wen model to simulate dynamic behavior of pot bearings in railway bridges. A fourt-order Runge-Kutta scheme with integration time steps down to 10^{-5} used to obtain accurate solutions.

2.4 FPBearingPTV element

In this study, 'FPBearingPTV'element (Kumar, 2017; Kumar et al., 2014) is used to model the CSS isolators in OpenSees. The element is modified version of another element in OpenSees library, called 'singleFPBearing' (Schellenberg, 2014). These elements use the Rate-independent plasticity model for constitutive equations and allow user to select the friction model that CSS element used with. The following discussions on 'FPBearingPTV'element that pertains modeling also applies for 'singleFPBearing' element.

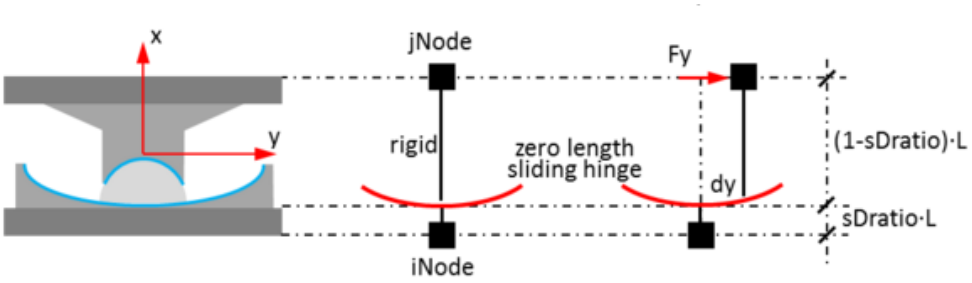

Figure 2-2. Section through ‘singleFPBearing’and‘FPBearingPTV’elements (Schellenberg, 2014).

‘FPBearingPTV’ element is defined by two nodes which correspond the free and fixed ends of the isolator. The iNode represents the sliding surface that atttached to a fixed base whereas the jNode represents the slider on which axial load applied. For each node, six degrees of freedom (DOF) is defined for axial properties. The consititutive model for shear deformations are based on the coupled Rate-independent plasticity, while the behavior of the axial (vertical) and rotational (bending and torsional) DOFs are defined by using a uni-axial material which defined by user. For shear DOFs, the force-displacement characteristic is automatically defined in to the element by program by using the mechanical properties of the isolator such as effective radius of curvature, initial stiffness in lateral direction, friction coefficient and axial load. Also, contact area of the slider and the mass of the isolator are set by user. The P-Delta moments are entirely transferred to the iNode through the shear distance parameter which defined as a fraction of the height of the element. The uplift behavior does not accounted for, thus in the event of tension acting on the axial DOF, the element axial force is set equals to zero automatically. An inherent viscous damping can be assigned to the element through Rayleigh damping, though it is not recommended for the CSS isolators, since it introduces an artificial viscous damping, called damping leakage, in the isolation system (Sarlis and Constantinou, 2010). The effect of the velocity, pressure and heating on the friction coefficient are accounted for by the element. The user can decide as to whether these effects are included in the friction model

for analyses. Alternatively, Coulomb friction model can be assigned to isolators by simply not including any of the aforementioned effects in friction model.

An information on modeling the CSS isolator for nonlinear response history analyses are given in the following. The behavior of the double CSS isolator is identical to single CSS isolator if the friction properties of two sliding interface are identical. The mechanical properties required for an analysis are the effective radius of curvature, R_{eff}, the yield displacement, D_{yield}, the friction coefficient for top and bottom sliding interfaces, μ_1, μ_2,the axial (vertical) stiffness, k_{vert}, the rotational, k_{rot}, and torsional stiffnesses, k_{tor}. It is assumed that both sliding interface have identical friction properties, $\mu_1 = \mu_2 = \mu$. In that case, the effective radius of curvature is equal to the sum of radii of curvature of two concave surface and modified for the height of the slider (Fenz and Constantinou, 2006).

$$R_{eff} = R_1 + R_2 - h \tag{2-20}$$

where R_1, R_2 are the radius of top and bottom concave surfaces respectively, h is the height of the rigid slider.

The axial (vertical) stiffness, k_{vert}, can be estimated as follows:

$$k_{vert} = 0.5\left(\frac{A_{slider}E_{steel}}{H}\right) \tag{2-21}$$

where A_{slider} is the slider area, E_{steel} is the elasticity modulus of steel, H is the height of the isolator. The constant 0.5 is used to account for isolator flexibility (Constantinou et al., 2011).

The rotational stiffnesses, k_{rot}, about two horizontal axes are speficified with a large number or fixed to avoid additional flexibility in the isolator (Constantinou et al., 2007) whereas the torsional stiffness, k_{tor}, is set to zero or near zero since the isolator have almost zero resistance to torsion. The yield displacement, D_{yield}, can be taken on the order of 1-2 mm. Furthermore, the rate parameter related to the effect of velocity on the friction coefficient is set half of that would be set for

single CSS isolator, as the velocity at sliding interface in double CSS is approximately half of what would occurs in single CSS isolator.

2.5 Friction coefficient

When a solid body in contact with another solid moves relative to the other, the friction force occurs. Adhesion, plowing and viscoelastic effects are mechanisms that results in friction (Constantinou et al., 2007). By definition, the friction coefficient is the ratio of the friction force to the normal force.

$$\mu = \frac{N}{F_f} \tag{2-22}$$

where μ is the friction coefficient; N, F_f are the normal and friction forces respectively.

Experiments on various types of sliding bearing and isolators used in seismic applications have revealed that the friction between the PTFE-type slider and stainless steel sliding surface do not behave according to Coulomb's law of friction in which friction coefficient is postulated as independent of sliding velocity and contact area (Tyler, 1977; Constantinou et al., 2007). Rather, it depends on various factors such as sliding velocity, contact pressure, surface temperature, load dwell, wear, surface condition, direction of lay of surface, of which three have found to be major influence on the response of the CSS isolators. These are the sliding velocity, contact pressure and the temperature at the sliding surface (Contantinou et al., 2007; Quaglini et al., 2012). The temperature effect is expected to be the most important factor that influences the friction coefficient during an earthquke event (Kumar et al., 2015).

The friction coefficient can be classified as static and dynamic. Static friction occurs at first initiation of motion of the slider (breakaway friction). It also occurs at momentarily stops of the slider. The latter especially is manifested at motion reversals of the slider during a cyclic motion. It also occurs due to stick-slip

behavior when the friction coefficient is large enough to produce a friction force greater than recentering force as well as when the concavity of the sliding surface (R_{eff}) is low.

The dynamic friction occurs when the slider moves with respect to its surface. The experiments on typical CSS isolators have showed that the static friction coefficient usually is larger than dynamic friction coefficient (Quaglini et al., 2012; McVitty and Constantinou, 2015), though the extent of the difference depends on the liner material used at the sliding interface. Moreover, there are studies which reported that the breakaway friction coefficient is smaller than the friction coefficient at high velocities (Mokha et al., 1990). In a experimental study, Mosqeuda et al. (2004) observed that the breakaway friction was pronounced only on unscragged sliders. A high breakaway friction coefficient can prevent the activation of the slider in a seismic event, leading significant increase in accelerations transferred to the superstructure through CSS isolators. However, at very low friction levels, the static friction have negligible effect on structure and can be ignored (Quaglini et al., 2018). In this study, the term friction coefficient indicates the dynamic friction coefficient unless stated otherwise.

Next, the nominal friction coefficient, μ_{nom}, for an CSS isolator is defined as the friction coefficient over three cycles of motion with maximum amplitude obtained from a displacement-controlled test (McVitty and Constantinou, 2015).

$$\mu_{nom} = \frac{\sum_{i=1}^{3} \mu_{ic,test}}{3} \tag{2-23}$$

μ_{nom} is friction coefficient averaged over three cycles of motion and, $\mu_{ic,test}$ is the friction coefficient at the ith cycle of motion obtained from test.

The nominal friction coefficient is of importance as it gives a single value about the friction property of the isolator under consideration. In design, the nominal friction coefficients are used within Equivalent Linear Force (ELF) method to estimate the displacement response and the effective translational period of the isolated

structure. The latter is of interest since the ground motions are scaled over a period range whose lower and upper bounds are calculated through ELF procedure.

In this study, μ, represents the instanteneous friction coeffficient in the isolator, and typically indicates the friction in response history analysis, whereas μ_{ic} represents the friction coefficient at ith cycle of motion, and is calculated by energy dissipation at respective cycle. Moreover, $\mu_{ic,test}$ represents the friction coefficient at ith cycle of motion, obtained from tests.

2.5.1 Effect of velocity on friction coefficient

The friction coefficient depends on the sliding velocity. In general terms, the friction coefficient increases as the sliding velocity increases. However, details on the subject slightly complicated than that. The friction coefficient can be significantly different at three states of the slider, namely, at initiation of motion, at low velocities, at high velocities. At the initiation of motion there is a breakaway friction which, mostly, is the highest value among all states. Then, immediately after the slider moves, the friction coefficient drops to its lowest level. This ocurs at very low velocities. Then, as the velocity increase, the friction coefficient increases up to a level beyond which the friction coefficient become invariable (Constantinou et al., 2007). The velocities that friction coefficient insensitive to velocity changes anymore are called high velocities and depends on the coating materials used at sliding interface. Thus, high velocity vary by manufacturer. The prototype tests with different sliding velocities should help to assess the high and low velocities for the isolator at hand. Typical examples for the lower bound of the high velocities for different CSS isolators in literature ranges 10 to 20 cm/sec (Constantinou et al., 1990; Gandelli, 2017). The relationship between the sliding velocity and the friction coefficient can be expressed as follows (Mokha et al., 1988)

$$\mu(v) = \mu_{high} - (\mu_{high} - \mu_{low})e^{-a|v|} \tag{2-24}$$

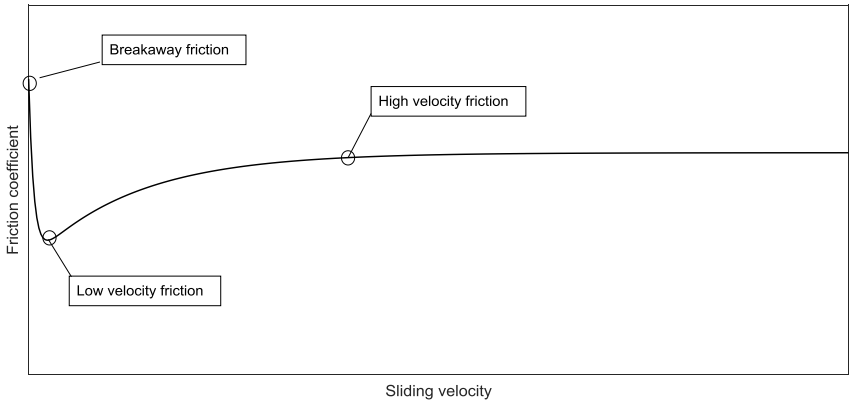

Figure 2-3. Typical sliding velocity-friction coefficient relationship of CSS isolator that have PTFE-stainless steel interface.

where μ is the estimated friction coefficient, μ_{high} is the friction coefficient measured at high sliding velocities (e.g. > 20 cm/sec), μ_{low} is the friction coefficient measured at low velocities (e.g < 2.5 cm/sec), a is the rate parameter that control the shape of the velocity-friction coefficient curve and v is the velocity at the sliding interface.

The parameters μ_{high}, μ_{low}, a are determined by means of prototype tests. The ratio of the friction coefficient at low velocity to the friction at high velocity, μ_{low}/μ_{high}, strictly depends on the material used for coating. Kumar et al. (2015) reported that the ratio vary significantly, ranging between 0.385 and 1.0 for different PTFE-based materials observed from past studies. A ratio of 1.0 indicates a friction coefficient insensitive to sliding velocity.

2.5.2 Effect of pressure on friction coefficient

Experimental studies on the sliding-based isolators with PTFE-stainless steel sliding interface have shown that the friction coefficient decreases asymptotically, as the contact pressure increases (Higoshino et al., 2003; Dolce et al., 2005; Constantinou et al., 2007). A theory on the relationship between the contact pressure and the friction coefficient is presented by Constantinou et al. (2007) and

summarized in the following. The shear strength, s, inthe PTFE-stainless steel interface can be expressed as follows:

$$s = s_o + \alpha p_r \tag{2-25}$$

where s_o is the shear strength at zero axial pressure, α is constant, p_r is the actual pressure acting on the interface.

The friction force, F_f, in the interface can be expressed by the following:

$$F_f = sA_r \tag{2-26}$$

where s is the shear strength in the interface, A_r is the actual (real) contact area.

The friction coefficient, by definition, is the ratio of the friction force to the compressive normal load on the interface. That is,

$$\mu = \frac{F_f}{N} \tag{2-27}$$

where all terms were defined previously.

The axial load can be expressed in terms of actual pressure and the actual contact area as follows:

$$N = p_r A_r \tag{2-28}$$

where all terms were defined previously.

Substituting the equations (2-25) (2-26) and (2-28) into (2-27), the following expression is obtained:

$$\mu = \frac{s_o}{p_r} + \alpha \tag{2-29}$$

where all terms were already defined.

Next, the actual pressure, p_r, is the pressure over the actual area of contact, A_r. That is,

$$p_r = \frac{N}{A_r} \tag{2-30}$$

where all terms were defined previously.

The apparent contact area is, as the name implies, the visible area of the mating surfaces (Bowden and Tabor, 1964). The actual contact area between two solid in contact can be significantly smaller than the apparent contact area, as the true contact occurs at regions called junctions that results from asperities across the contact surfaces. For PTFE-stainless steel sliding interfaces, the actual contact area is equal to the apparent contact area of the CSS isolator, which is equal to the area of the slider (Constantinou et al., 2007). Therefore, the equation (2-29) can be expressed as follows:

$$\mu = \frac{s_o}{p} + \alpha \tag{2-31}$$

whereμ is the friction coefficient,p is the apparent pressure acting on the sliding interface and other terms were defined earlier. The apparent pressure, p, can simply be calculated as follows:

$$p = \frac{N}{A} \tag{2-32}$$

where N is the axial force on the isolator and the A is the area of the slider of the isolator.

The apparent pressure obtained from last equation is also called ‘average’ pressure in literature. The reason for this is due to fact that the pressure acting on the slider is not uniformly distributed as the resultant force of the pressure on the sliding interface must be off center to satisfy moment equilibrium (Fenz et al., 2008b). In this study, the average and apparent contact pressure acting on the isolator is denoted as ‘apparent contact pressure’ or ‘contact pressure’ for brevity.

The friction coefficient decreases as the pressure increases. However, Mokha et al. (1990) noted that there is a certain level beyond which the friction coefficient does not depends on the contact pressure. This level depends on the type of the coating material used within the CSS isolator. Hence, it is required to have a number of prototype tests performed under a wide range of contact pressures to be able to develop the pressure-friction coefficient relationship accurately.

Various formulations have been used over the years to define the pressure-friction coefficient relationship for the CSS isolators. Chang et al. (1990) used the following equation:

$$\mu(p) = \frac{1}{\lambda_1 + \lambda_2 p} \tag{2-33}$$

where μ is the dynamic friction coefficient, p is the average pressure, $\lambda_1, \lambda_2 > 0$ are the constants determined by tests.

Tsopelas et al. (1994) proposed the following relationship:

$$\mu_{high}(p) = \mu_{high,0} - (\mu_{high,0} - \mu_{high,p})\tanh(\epsilon p) \tag{2-34}$$

where μ_{high} is the friction coefficient at high velocities, $\mu_{high,0}$ is the friction coefficient at high velocities measured under almost zero average pressure, $\mu_{high,p}$ is the friction coefficient at high velocities measured under very high pressures, ϵ is the calibration parameter.

The European standart for anti-seismic devices, EN 15129 (CEN, 2009) recommends the following equation:

$$\mu(p) = \frac{c}{\sqrt{p}} \tag{2-35}$$

where c is the experimental constant and p is the average contact pressure.

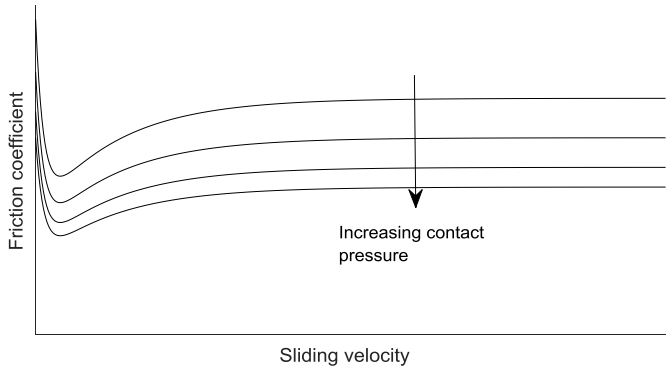

Figure 2-4. Typical sliding velocity-friction coefficient relationship for different contact pressures of CSS isolator.

2.5.3 Effect of temperature and frictional heating on friction coefficient

Past studies have shown that the temperature at the sliding interface has major influence on the friction coefficient (Constantinou et al., 2007; Quaglini et al., 2012). The friction coefficient decreases as the temperature at the sliding interface increases. Recent studies have shown that temperature is the most important factor on response quantities such as peak displacement and peak acceleration during an earthquake (Kumar et al., 2015). The variation in the friction coefficient due to temperature is attributed to change in viscoelastic properties of PTFE (Constantinou et al., 2007). The temperature at sliding interface changes due to (1) change in ambient temperature, (2) frictional heating.

Quaglini et al. (2012) have conducted a series of tests on CSS isolators with PTFE type coating material, at external temperature ranges between -35 to 35°C. They reported both the breakaway and dynamic friction coefficients increase as the external temperature decrease with rate of changes that differs at the low and high temperatures. Although low ambient temperature can have significant effect on the breakaway and the friction coefficient at low velocities, it has a mild effect on the friction coefficient at high velocities, since the frictional heating that occurs at high velocity of sliding modarates the effect of low temperature (McVitty and Constantinou 2015). The ambient temperature is not considered in the friction models or in the response history analyses, however, its effect can be included indirectly through property modification factors when the lower and upper bound properties of the isolator are determined.

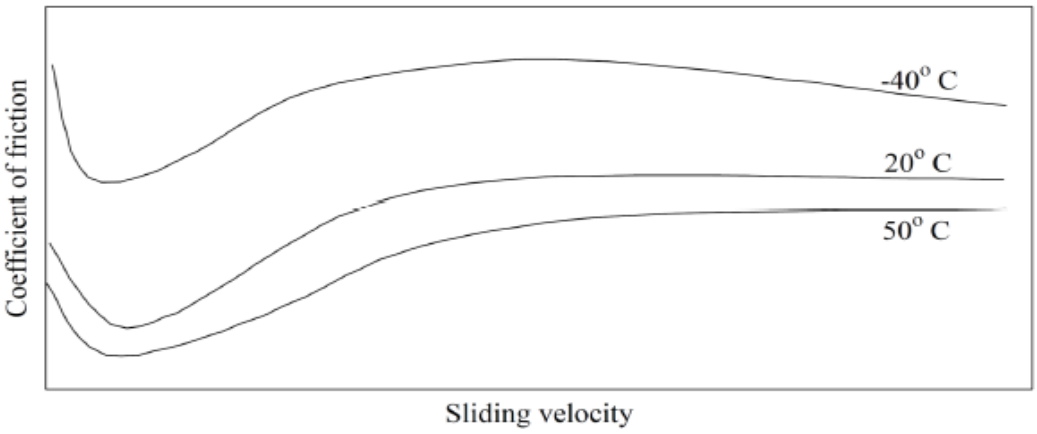

Figure 2-5. Schematic for the effect of the temperature on the friction coefficient (Kumar et al., 2015).

The temperature at sliding interface increases due to frictional heating. Moroever, the friction coefficient returns quickly to its original value that measured before the heating effect is manifested, once the motion stops. In other words, the heating effect on friction coefficient is neutralized as the sliding interface cools off. This is of importance not just because the temperature rise due to frictional heating is substantial, but also this temperature diffuses quickly into the surrounding medium (McVitty and Constantinou 2015).

Past studies have showed that the decrease in the friction coefficient while the increase in the number of cycles follows a negative exponential trend (Dolce and Cardone 2005), due to a phenomenon called ‘thermal control of friction’ (Quaglini et al., 2014) which explained in the following. The heat generated at the sliding interface depends on various factors including the friction coefficient. Thus, the decrease in the friction coefficient limits the further increase in the heat flux. Essentially, the temperature at the sliding interface depends on two factors, namely, the path of slider (or prior heating surface) and the instanteneous heat flux. The heat flux is proportional to the coefficient of friction, contact pressure and velocity of sliding. Furthermore, the composition of the sliding interface, which typically proprietary, affects the relation of friction coefficient and the heating (ASCE, 2016). The experimental studies on the CSS isolators that have unlubricated,

PTFE-stainless interface have shown that the decrease in friction coefficient on the order of 20% (Constantinou et al., 2011). In an experimental study, Mosqueda et al. (2004) measured decrease in the friction coefficient on the order of 20% after 3 cycle of loading at peak velocities larger than 12.7 cm/sec under pressures about 50 to 90 MPa, for Friction Pendulum isolator that have PTFE-stainless steel interface. Dolce and Cardone (2005) found decrease in the friction coefficient on the order of 25-30% after 5 cycle of loading for PTFE-steel interfaces. Quaglini et al. (2012) observed 18% decrease in the friction coefficient after 3 cycle in a test using the CSS isolators.

The effect of frictional heating is accounted for in the codes. According to EN 15129 (2009), the design displacement, maximum lateral force and energy dissipated per cycle must deviate less than 15% from their nominal values in three cycles of loading. ASCE 7-16 (2016) do not give a limit on the decrease in the friction coefficient due to heating effects, though, it rewards the CSS isolator by allowing not to use the property modification factor associated with the heating effect if the effect of heating is accounted for in response history analysis.

Constantinou et al. (2007) present a theory for the frictional heating in sliding based isolators that have PTFE-stainless steel interface. According to that study, the temperature rise, ΔT, at a given point on the sliding surface at time t can be calculated using the following equation (Kumar et al., 2013):

$$\Delta T(x,t) = \frac{\sqrt{D}}{k\sqrt{\pi}} \int q(t-\tau) \exp\left(-\frac{x^2}{4D\tau}\right) \frac{d\tau}{\sqrt{\tau}} \tag{2-36}$$

where x is the depth measured from the sliding surface, D is the thermal diffusivity of steel, k is the thermal conductivity of steel, q is the heat flux and calculated by as follows:

$$q=\mu v p \tag{2-37}$$

where μ is the friction coefficient, v is the slider relative velocity, p is the apparent contact pressure. As shown from equation (2-37), the pressure indirectly affects the friction coefficient by contributing the heat flux. This is supported by an

experimental study on Friction Pendulum Isolator. Travato (2013) used thermographic camera to monitor the temperature rise at sliding interface when the slider in motion, and found that the pressure have a strong impact on temperature rise. According to the study, the flash temperature measured at sliding interface under a pressure of 45 MPa is double that measured with a pressure of 8 MPa.

In analysis, the friction model adjusts the friction coefficient according to temperature information. This is accomplished by monitoring a set of points located on sliding surface. The temperature rises at a monitored point when the heat flux generated at respective point, which occurs if that point falls within the area enclosed by slider. That is, equation (2-37) holds for a monitoring point on sliding surface, if that point falls below the slider at that time. A number of monitoring points uniformly distributed on sliding surface are required for this purpose. Then, the temperature data at any time given for friction model is calculated as the average value of the points directly below the slider. For the ease of computation, the numerical model, instead, only monitors the center of sliding interface to track the temperature data, as two approaches approximately give the same results on the temperature (Kumar et al., 2015).

2.6 Friction model used in this study

The friction model with which CSS element used in this study is described in the following. 'FPBearingPTV' element simultaneously accounts for the velocity, pressure and heating effect on the coefficient of friction based on predefined relationships. The equations for these relationships are based on the work of Kumar et al. (2015) and might not be apply for different studies. However, the source code of the element along with the program OpenSees is available and users can compile an executable OpenSees program according to their own interest. Such a procedure is employed in this study. The experimental results on isolators that will be described in the Chapter 5 have been used to define a new set of equations to account the velocity, pressure and heating effect on friction. Then, a new OpenSees

program have been compiled and used for time history analyses.A brief description on procedure of calculation of the friction coefficient in OpenSees is presented in the following. The coefficient of friction is adjusted by the program at each time step of analysis according to (1) sliding velocity, (2) apparent pressure, (3) temperature at sliding interface through following equation

$$\mu(v, p, T) = \mu_{ref}(k_v(v))(k_p(p))(k_T(T)) \quad (2\text{-}38)$$

where μ is the instanteneous coefficient of friction, μ_{ref} is the reference friction coefficient, $(k_v(v))$, $(k_p(p))$ and $(k_T(T))$ are the factors to account for velocity, pressure and heating effect respectively and they are function of respective effect; v, p and T are the instanteneous values of the sliding velocity, contact pressure and temperature of sliding interface.

The reference friction coefficient, μ_{ref}, is a friction coefficient measured experimentally under a known (reference) contact pressure, called p_{ref}, and known (refence) temperature of sliding interface, called T_{ref}, and also measured at high velocity of sliding (e.g. v> 200 mm/sec). The reference temperature of sliding interface, T_{ref}, is assumed be $20°C$. Thus, essentially, μ_{ref}, is the friction coefficient at the beginning of high velocity of sliding, measured before heating effect is manifested, and is obtained through a dynamic test performed under a known contact pressure. The factor $k_v(v)$ is a function of sliding velocity and is calculated through an equation that describes the relation of instanteneous friction coefficient with sliding velocity. The factor $k_p(p)$ is a function of contact pressure and is calculated through an equation that describes the relationship between instanteneous friction coefficient at high velocity and apparent contact pressure. The factor $k_T(T)$ is a function of temperature at sliding interface and is calculated through an equation that relates instanteneous friction coefficient at high velocity with the temperature at sliding interface.

2.6.1 Velocity effect

The effect of velocity on the friction coefficient is accounted for by following equations (Kumar et al., 2015):

$$\mu(v) = \mu_{ref}(k_v(v)) \tag{2-39}$$

$$k_v(v) = 1 - \left[\left(1 - \frac{\mu_{low}}{\mu_{high}}\right)\exp(-\alpha|v|)\right] \tag{2-40}$$

where μ is the coefficient of friction for given sliding velocity v, μ_{ref} is the reference coefficient of friction, $k_v(v)$ is the parameter of velocity effect, μ_{high} is the coefficient of friction measured at high velocity of sliding (e.g. v > 200 mm/sec), μ_{low} is the coefficient of friction measured at low velocity of sliding (e.g v < 25 mm/sec) and α is the rate parameter that determines shape of the velocity-coefficient of friction curve.

2.6.2 Pressure effect

The effect of the contact pressure on the coefficient of friction is accounted for by following equations (Kumar et al., 2015):

$$\mu(p) = \mu_{ref}(k_p(p)) \tag{2-41}$$

$$k_p(p) = c_1\left(c_2^{c_3 \cdot p} + c_4\right) \tag{2-42}$$

where μ is the coefficient of friction for given apparent contact pressure p (compressive), μ_{ref} is the coefficient of friction measured at high velocity, under known contact pressures and at known temperature at sliding surface, c_1, c_2, c_3, c_4 are the parameters that determine shape of the pressure-friction coefficient curve.

2.6.3 Heating effect

The effect of frictional heating on the friction coefficient is accounted for by means of temperature at the sliding interface. To this end, the following equations are used (Kumar et al., 2015):

$$\mu(T) = \mu_{ref}(k_T(T)) \tag{2-43}$$

$$k_T(T) = \phi\left(b^{\frac{T}{c}} + d\right) \tag{2-44}$$

$$\phi = \left(b^{(T_{ref}/c)} + d\right)^{-1} \tag{2-45}$$

where μ is the coefficient of friction for a given temperature at sliding interface T, μ_{ref} is the coefficient of friction measured at high velocity and under known contact pressure p_{ref} and at known temperature at sliding surface, T_{ref},b, c, d, ϕ are parameters that determine the shape of temperature- friction coefficient curve.

2.6.4 Combined effect of velocity, pressure and heating

In equation (2-38), the instanteneous friction coefficient is expressed as a product of a reference friction multiplied by factors related to velocity, pressure and heating effect. These factors are adjusted by program at each time step in analysis based on the state of isolator. Thus, the equation provides a means to observe the extent of each effect on friction separately during the course of motion in analysis. For example, a case where $k_v = k_p = k_T = 1.0$ being constant throughout the analysis indicates that the friction coefficient in isolator is constant, that is Coulomb friction model is assumed. As a second example, suppose that, for an isolator, $k_v = 0.5, k_p = 0.7$ and $k_T = 1.0$ at the beginning of analysis ($t = 0.0$ sec), and $k_v = 1.0, k_p = 1.5$ and $k_T = 0.5$ are calculated at a time, say $t = 9.0$ sec, in analysis. It can be inferred based on these data that (1) at low velocities, the friction coefficient is half of what would measured at high velocities, (2) the temperature at sliding interface is equal to reference value, $T_{ref} = 20°C$, (3) the apparent pressure on the

isolator at rest is higher than the refence pressure, p_{ref}, since k_p is lower than 1.0, (4) isolator is in motion with a high velocity at $t = 9.0$ sec, as $k_v = 1.0$, (5) the instanteneous apparent pressure acting on the isolator at $t = 9.0$ sec is lower than the refence value, p_{ref}, since k_p is higher than 1.0, (6) the pressure effect contribution tends toincrease the friction coefficient by a factor of 2.14 (1.5/0.7=2.14) at $t = 9.0$ sec, (7) the frictional heating tends to decrease the friction coefficient by a factor of 0.5 at $t = 9.0$. Therefore, the friction coefficient in the isolator would be calculated as 0.75 times the reference friction coefficient (1.0x1.5x0.5=0.75) at $t = 9.0$ sec for this hypothetical analysis.

CHAPTER 3

DESCRIPTION OF STRUCTURES USED IN ANALYSES

This study contains experimental and numerical studies on a seismically isolated hospital structure located in Izmit, Turkey. The finite element model of the structure is developed through the Sap2000 and OpenSees. The model differs from that of designed by project engineers in order to simplify modeling. The model will be referred as 'Model A' throughout the study and it will be used as a reference for two additional models which developed as an extension of 'Model A'. A brief information about the models used is given as follows. 'Model A' is the refence model from which other models are developed. Most of the discussions pertaining the importance of friction model will be based on the analyses performed using 'Model A'. It contains three superstructures mounted on top of a rigid base supported by total 234 isolators. The block heighest from base level has 7 storey is called block A. 'Model B' is a simple extension over 'Model A'. It contains the same three superstructure as those of 'Model A'. The only difference between 'Model A' and 'Model B' is that the block A in 'Model B' has 13 storey. This property makes 'Model B' more slender than 'Model A' and increases the eccentricity in the system with respect to the reference model. The number of isolators in the system 234 as well. 'Model C' consist of four 'Model A' that simply replicated to create a model that have T shape form in plan. Overall, 12 superstructures shares a common rigid base supported by total 898 isolators.

3.1 Key structure parameters

The past studies have shown that the torsional response of an isolated structure is affected by number of factors such as the isolation system eccentricity, the slenderness of structure, flexibility of isolation system and superstructure.

3.1.1 Isolation system static eccentricity

The center of rigidity of the isolation system is defined as the point at which a force can pass through in any horizontal direction without producing torsion (Kelly, 1997). The isolation system eccentricity is defined as the distance from the center of rigidity to the center of mass of the isolation system. For a CSS-based isolation system, the lateral resisting force is linearly proportional to the instanteneous axial load on the isolators. This feature provides a constant shift in the center of rigidity (CR) along with the center of mass (CM) during a seismic event (Becker et al. 2012). If all CSS isolators within a system have identical geometric and friction properties and are subjected to the same displacement, then the total lateral resisting force of the system can be expressed as a constant times the supported weight (Skinner et al., 2011). However, this is extremely unlikely for the reason explained in the following. The friction coefficient of two identical isolator can differ significantly due to differences in instantenous axial loads on them that might occurs during the course of motion. This will induce eccentricity in the isolation system. Hence, although the CR shifts with CM of the isolation system during the motion, some amount of eccentricity will be present due to constant variations in friction coefficients.

The isolation system static eccentricity, in this study, is defined as the distance from CM to CR when the system at rest. It can be calculated as follows (Kelly, 1997) :

$$e_x = \frac{1}{K_y}\sum_{i=1}^{m} k_y^i x_i \tag{3-1}$$

$$e_y = \frac{1}{K_x}\sum_{i=1}^{m} k_x^i y_i \tag{3-2}$$

$$e = \sqrt{e_x^2 + e_y^2} \tag{3-3}$$

where e_x, e_y are the eccentricities in horizontal principal directions x, y; e is isolation system static eccentricity, m is the number of isolators in the system, x_i,

y_i are the location of the ith isolator from the center of mass in principal directions, k_x^i, k_y^i are the stiffness of the ith isolator in principal directions and K_x, K_y are the total stiffness of the isolation system in principal directions, calculated as follows:

$$K_x = \sum_{i=1}^{m} k_x^i \tag{3-4}$$

$$K_y = \sum_{i=1}^{m} k_y^i \tag{3-5}$$

where all terms already defined.

The static eccentricity alone does not provide meaningful information on the extent to which torsional response is amplified. Thus, it is usually normalized either by longest plan dimension or by radius of gyration of the isolation system (Nagarajaiah et al., 1993). In this study, both of these parameters are presented:

$$\frac{e}{r} = \frac{\text{Static eccentricity of the isolation system}}{\text{Radius of gyration of the isolation system}} \tag{3-6}$$

$$\frac{e}{L_{max}} = \frac{\text{Static eccentricity of the isolation system}}{\text{Longest plan dimension of the structure}} \tag{3-7}$$

The radius of gyration of the isolation system is calculated as follows:

$$r = \sqrt{\frac{I}{M}} \tag{3-8}$$

where I is the mass moment of inertia of the isolation system and M is the total mass supported by isolation system. Furhermore, the mass moment of inertia can be calculated as follows:

$$I = \sum_{i=1}^{m} m_i(x_i^2 + y_i^2) \tag{3-9}$$

where m_i is the mass supported by ith individual isolator and x_i, y_i are the coordinates of that isolator with respect to center of mass.

3.1.2 Slenderness of structure

The past studies have shown that the slenderness of a structure isolated with CSS isolators has influence on torsional response (Almazan, 2003). The torsional amplifications increase with larger slenderness ratios which defined as follows:

$$\gamma = \frac{H}{L_{min}} \tag{3-10}$$

where γ is the slenderness ratio, H is the height of the structure above the isolation base and L_{min} is the shortest plan dimension of the structure.

3.1.3 Flexibility of isolation system

The effective translational period of the isolation system, T, is defined as the first uncoupled period of the isolated structure, which can be calculated as follows:

$$T = 2\pi \sqrt{\frac{M_{total}}{K_{eff,total}}} \tag{3-11}$$

where M_{total} is total mass of the superstructures (i.e., total mass supported by isolation system), $K_{eff,total}$ is the total lateral stiffness of the isolation system in one of the principal horizontal directions. That is, $K_{eff,total}$ is calculated using either equation (3-4) or (3-5).

The effective torsional period of the isolation system, T_θ, is defined as the first uncoupled torsional period of the isolated structure, which can be calculated as follows:

$$T_\theta = 2\pi \sqrt{\frac{M_{total} r^2}{K_\theta}} \tag{3-12}$$

where r is the radius of gyration of the isolation system, which can be calculated using equation (3-8); K_θ is the effective torsional stiffness of the isolation system which can be calculated using following equation:

$$K_\theta = \sum_{i=1}^{n} k_x^i \, y_i^2 + \sum_{i=1}^{n} k_y^i \, x_i^2 \tag{3-13}$$

where k_x^i, k_y^i are the stiffnesses of the ith isolator in the principal horizontal directions, x_i, y_i are the coordinates of the ith isolator with respect to center of mass.

The ratio of effective translational period to the effective torsional period is denoted as Ω_θ.

$$\Omega_\theta = \frac{T}{T_\theta} \tag{3-14}$$

The value Ω_θ greater than unity indicates a torsionally stiff system, yet the isolated structures usually have Ω_θ values closer to unity. An experimental study showed that there is tendency for increase in torsional amplifications with lower Ω_θ values (Wolff et al., 2014).

Table 3-1. Key structure parameters of the models used in this study.

Model tag	Number of isolators	Slenderness ratio	Eff. translational period	Transl. to torsion.	Plot
-	n	γ	T [sec]	Ω_θ	-
Model A	234	0.38	3.84	1.02	Figure 3-1
Model B	234	0.65	3.84	1.04	Figure 3-2
Model C	898	0.36	3.84	1.00	Figure 3-5

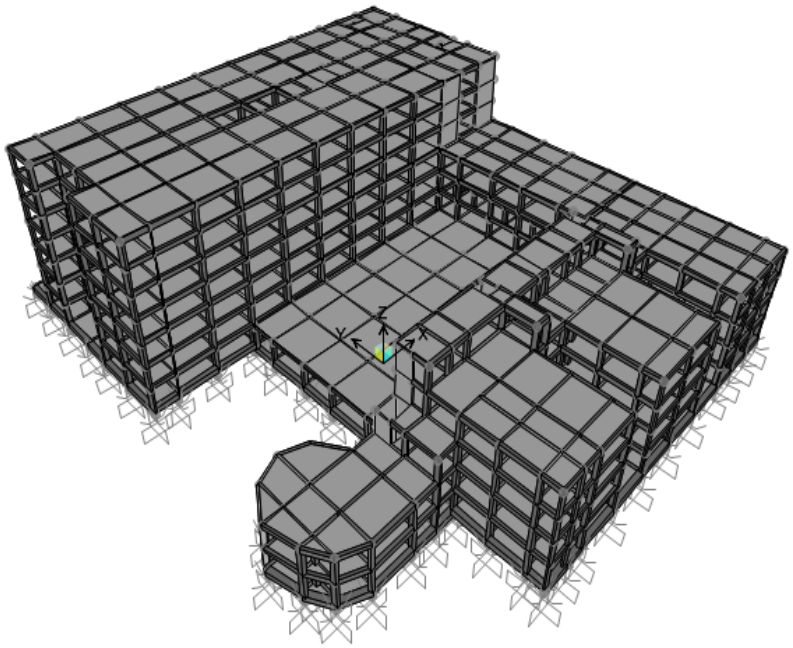

Figure 3-1. Three-dimensional view of the hospital structure used in analyses. This model is referred as ‘Model A’.

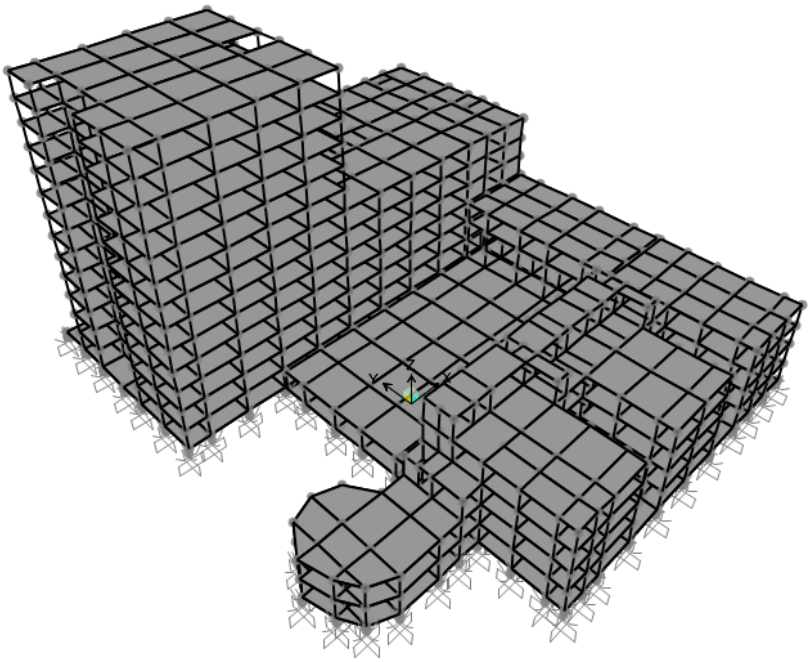

Figure 3-2. Three-dimensional view of ‘Model B’.

3.2 Description of Model A and Model B

The reference stucture consists of three reinforced concrete superstructures (blocks) mounted on top of common rigid base supported by isolation system. The plan view of the isolation level is shown in Figure 3-3 where each blocks can be seen. Shear walls and frame elements constitute the structural system along with double CSS isolators. The structure have 92 x 107 m in plan dimensions. For 'Model A', heighest level is 34.5 meters (block A) whereas for Model B, the heighest level is 59.8 meters from isolation base.The storey heights are 4.5 m. The dimensions of the shear walls, columns and beams are varying along the structure with typical beam dimensions are 50 cm x 80 cm while typical column dimensions are 80 cm x 80 cm and typical shear wall thicknesses are 30 cm. The isolation system consists of 234 double CSS isolators. The isolation system layout is shown in Figure 3 4.

Torsional response of an isolated structure can be measured by monitoring the corners isolators, since the torsion amplify displacements at corner isolators with respect to interior isolators. Selected isolators are presented on Table 3-2.

Table 3-2. Isolators selected for time history analyses.

isolator tag	location (see Figure 3-4)
129	Center of Rigidity
222	Corner 1
234	Corner 2
1	Corner 3
11	Corner 4
53	Corner 5

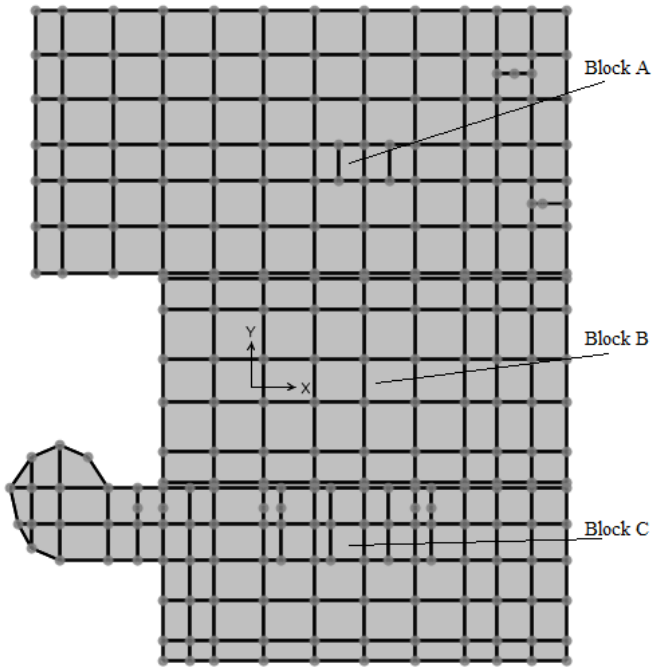

Figure 3-3. Plan view of the isolation level for Model A and Model B.

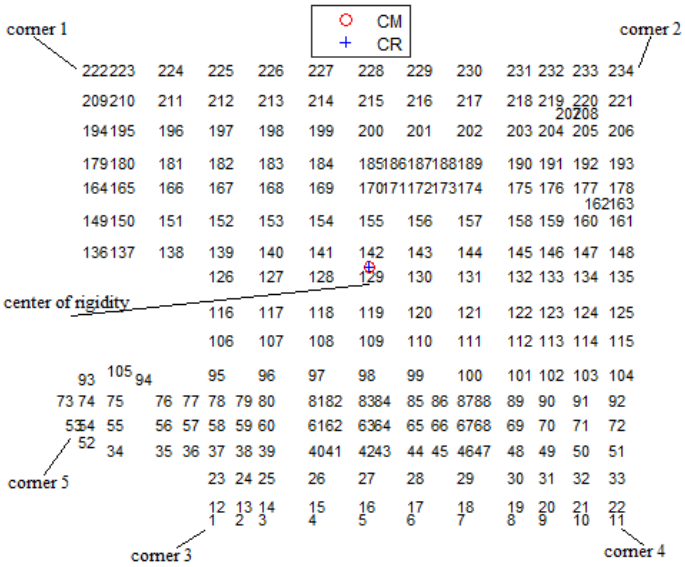

Figure 3-4. Isolation system layout of ‘Model A’ and ‘Model B’ with isolator labels.

3.3 Description of Model C

‘Model C’contains 12 superstructures mounted on a rigid base supported by total 898 isolators. It has been developed by four ‘Model A’ which replicated to form Model C with a T shape plan and setbacks in elevation. The plan dimensions are 168 x 335 meters while at the heighest level 59.8 meters above the base, corresponding to 13 storeys. Although it is not shown here, for the reasons explained for ‘Model A’ and ‘Model B’, six isolators are selected to monitor the response of the structure during the course of analyses, of which five from corners and one from center of rigidity.

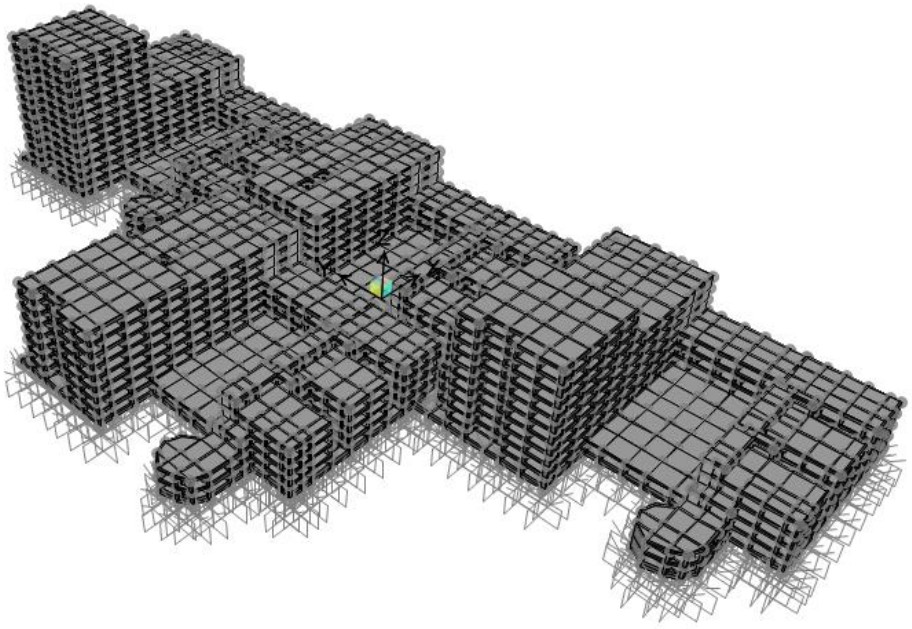

Figure 3-5. Three-dimensional view of the Model C.

3.4 Equivalent Linear Force procedure

Equivalent Linear Force (ELF) procedure is utilized to obtain an estimate for displacement, effective period and effective damping. The effective period of the isolation system is determined for lower and upper bound properties of the isolation system seperately to account for variations in these properties associated with uncertanties in various factors such as manufacturing and environment. For a CSS based isolation system, the variations in the isolation system properties is associated with only uncertainties in the friction coefficient, given that isolators can be constructed with a high degree of geometric precision. The other importance of the effective period is that it is used to scale the ground motions selected for response history analyses.

The ELF procedure described in the next is adapted from McVitty and Constantinou (2015), applies for CSS-based isolation system, and is used to determine, for upper and lower bounds, the effective period of the isolated structures used in this study. In the ELF method, the isolated structure is treated as SDOF system having a weight equal to the total weight of the structureand a lateral stiffness equal to the total lateral effective stiffness of the isolation system.

$$T_{eff} = 2\pi \sqrt{\frac{W_{total}}{gK_{eff,total}}} \tag{3-15}$$

where W_{total} is the total seismic weight of the isolated structure (including the weight of isolation system), $K_{eff,total}$ is the total effective stiffness of the isolation sytem, g is the gravity constant.The total effective stiffness of the isolation system can be synthesized by

$$K_{eff,total} = K_{p,total} + \frac{Q_{total}}{D_d} \tag{3-16}$$

where $K_{p,total}$ is the total post-yield (or sliding) stiffness, Q_{total} is the total characteristic strength of the isolation system, and D_d is the design displacement at center of mass of the isolation system obtained through ELF procedure.

The total post-yield stiffness, $K_{p,total}$, can be calculated as follows, if all isolators have same R_{eff}.

$$K_{p,total} = \frac{W_{total}}{R_{eff}} \tag{3-17}$$

where all terms are already defined.

The total characteristic strength of the isolation system, Q_{total}can be calculated as follows:

$$Q_{total} = \frac{\mu_{system} W_{total}}{D_d} \tag{3-18}$$

where μ_{system} is the friction coefficient of the isolation system and W_{total} is the total structure weight,D_d is the design displacement obtained through ELF procedure.The μ_{system} is a single value that represents the friction property of the isolation system, and can be taken as the weighted average friction coefficient of the isolation system (McVitty and Constantinou, 2015). The calculation of the μ_{system} is especially important for large structures where significant variations in friction coefficient among individual isolators are pronounced due to large differences in contact pressures, as mentioned previously. It is common in design practice that the isolators are separated into groups based on their static axial loads, and the isolator size (e.g. slider area and height) that unique for each group is designed. For those cases, the friction coefficient representative of the entire system, μ_{system}, can be calculated with a weighted average approach as follows:

$$\mu_{system} = \frac{\sum_{i=1}^{nGroup} m_i \mu_{g,i} N_{avg,i}}{\sum_{i=1}^{nGroup} m_i N_{avg,i}} \tag{3-19}$$

where nGroup is the number of groups in the isolation system (or equivalently, number of different CSS isolator types in the system), m_i is the number of isolators in the ith group, $\mu_{g,i}$ is the friction coefficient that represents the ith group and $N_{avg,i}$ is the axial loadfor the ith group calculated by taking an average of the axial loads on the isolators in the respective group.

Typically, the friction coefficient for a group, $\mu_{g,i}$, is obtained from prototype tests in which the isolator from a group is subjected to the axial load similar to that expected under static condition.

Furthermore, the effective damping can be obtained as follows:

$$\beta_{eff} = \frac{4Q_{total}\left(D_d - D_{yield}\right)}{2\pi K_{eff,total} D_d^2} \tag{3-20}$$

where β_{eff} is the effective damping ratio of the isolation system, D_{yield} is the yield displacement of the isolation system and other terms are previously defined.

The damping reduction coefficient, B, can be obtanied by reading appropriate value from Table 17.5-1 in ASCE 7-16.

The design displacement, D_D, at center of mass of the isolation system can be determined as follows:

$$D_D = \left(\frac{g}{4\pi^2}\right)\left(\frac{S_1 T_{eff}}{B}\right) \tag{3-21}$$

where S_1 is the spectral acceleration value at a period of 1 seconds for 5% damped target spectrum and other terms are already defined.

The ELF procedure is implemented, separetely, to determine upper and lower bound properties of the isolation system. Only the friction coefficient is adjusted for this purpose as mentioned before. The nominal friction cofficient can be used for thelower bound value (McVitty and Constantinou, 2015) as it results in higher (i.e. unconservative) displacement response whereas the friction coefficient measured at first cycle can be used for upper bound. For lower bound, a factor of 0.85 is applied additionally for production tolerance whereas a factor of 1.16 is applied for upper bound to account for combined effect of aging and contamination.

3.5 Vibration characteristic of the isolation systems

The structures used in this study have been analyzed for different isolation system layouts. Each layout in a model differs only in terms of the number of groups (i.e. isolator types) used in the isolation system. For each layout in a model, the nominal friction coefficient that representative of the entire isolation system was almost same, as will be shown in later chapters. Furthermore, same effective radius of curvature was used for each group for each layout. Therefore, the vibration characteristic of the isolation system for each layout is almost identical, owing to fact described in the following. The effective period of the isolation system depends on the total effective stiffness as already given in equation (3-15). The total effective stiffness of the isolation system can be expressed as follows:

$$K_{eff,total} = \frac{W_{total}}{R_{eff}} + \frac{\mu_{system} W_{total}}{D_d} \tag{3-22}$$

where W_{total} is the total structure weight, R_{eff} is the effective radius of curvature, μ_{system} is the friction coefficient of the entire isolation system, D_d is the design displacement. Substituting the last equation into equation (3-15):

$$T_{eff} = 2\pi \sqrt{\frac{1}{g\left(\frac{\mu_{system}}{D_d} + \frac{1}{R_{eff}}\right)}} \tag{3-23}$$

where g is the gravity constant and other terms were defined previously. Note that, the period does not depend on the weight of the supported structure. The design displacement depends on isolator type and elastic design spectrum associated with seismic condition of the site. Since the same friction and the same effective radius of curvature have been used in the isolators for each isolation layout and for each model analyzed, the effective period of the structures were almost identical for the structures.

The vibration characteristics of the structures obtained through ELF procedure are presented on Table 3-3.

Table 3-3. Vibration characteristics of the isolated structures used in the study obtained from ELF procedure.

Property	Symbol	Model tag		
		Model A	Model B	Model C
Total structure weight [kN]	W_{total}	884744	1047473	3734461
System friction coefficient (nominal)	μ_{system}	0.049	0.049	0.05
System friction coefficient (first-cycle)	$\mu_{1c,system}$	0.057	0.057	0.058
Lower bound properties				
Friction coefficient for system	$0.85\mu_{nom,system}$	0.042	0.042	0.043
Total effective stiffness [kN/m]	$K_{eff,total}$	245691	259547	930787
Effective translational period [sec]	T_{eff}	4.02	4.03	4.02
MCE design displacement [m]	D_d	0.51	0.51	0.51
Effective damping ratio	β_{eff}	0.21	0.21	0.21
Upper bound properties				
Friction coefficient for system	$1.16\mu_{1c,system}$	0.066	0.066	0.067
Total effective stiffness [kN/m]	$K_{eff,total}$	267382	314901	1132643
Effective translational period [sec]	T_{eff}	3.65	3.66	3.64
MCE design displacement [m]	D_d	0.42	0.42	0.42
Effective damping ratio	β_{eff}	0.28	0.28	0.29

CHAPTER 4

GROUND MOTIONS USED IN ANALYSES

Seven ground motion records will be used for response history analyses. A site-specific target spectrum was available for the hospital structure. The ground motions are selected and scaled through PEER (Pacific Earthquake Engineering Research Center) strong motion database. The ground motions are amplitude scaled such a way that the mean of the SRSS scaled response spectrum of ground motions are not less than the 5% damped target spectrum in the period range of $[0.75T_u, 1.25T_l]$, where T_u, T_l are the fundamental periods of the isolated structure using upper and lower bound properties of the isolation system, respectively, per ASCE 7 (2016). The vibration characteristics of the structures analyzed in this study are almost identical. Thus, lower and upper bounds of the period of interest are calculated respectively as $0.75T_u = 2.73$ and $1.25T_1 = 5.04$ sec.

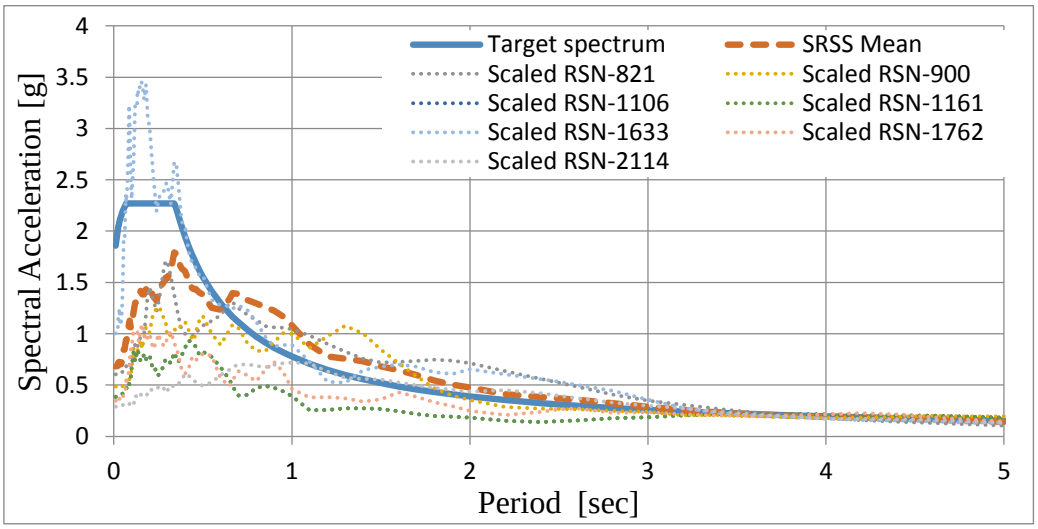

Figure 4-1. Target and Mean Spectra along with scaled ground motions used in analyses.

Table 4-1. Selected ground acceleration records with scale factors.

GM no	RSN*	Event	Year	Magnitude	Scale
1	1106	Kobe	1995	6.9	1.54
2	1161	Kocaeli	1999	7.5	1.29
3	1633	Manjil	1990	7.4	1.38
4	1762	Hector Mine	1999	7.1	1.20
5	2114	Denali	2002	7.9	0.65
6	821	Erzincan	1992	6.7	0.96
7	900	Landers	1992	7.3	1.68

*RSN: Record Sequence Number in PEER NGA-2 database.

CHAPTER 5

PARAMETER CALIBRATION

The parameters to account for velocity, contact pressure and heating effects on friction coefficient introduced in Chapter 2 are calibrated through the test data extracted from prototype tests conducted on DCSS isolators used in a hospital structure. The tests were performed by manufacturer and an independent test center. The testing setups were capable of toimpose peak displacement ± 50 cm in horizontal axis, with apeak force 40000 kN in vertical axis. The testing program involved a series of displacement-controlled, uni-directional, tests that carried out under a range of vertical loads. In a typical test, the DCSS specimens were subjected to combined application of a vertical compressive load and of a horizontal sinusoidal motion.

There are two approachs to determine the coefficient of friction from an displacement-controlled uni-directional test. These are explained briefly in the following. The first approach utilizes the digitally recorded force-displacement data obtained during the course of motion. With this approach, the friction coefficient at a specific time of the test can be extracted from recorded data. At each time instant, the friction force is calculated from the total measured force by eliminating the restoring term. In a displacement-controlled test, total measured horizontal force is the force required for actuators to impose the prescribed displacement to isolator at a specific time instant. By subtracting the recentering force from the measured actuator force, the friction force can be obtained.

$$F_{\mu}(t) = F(t) - \frac{N(t)}{R_{eff}} u(t) \tag{5-1}$$

where F_μ is the friction force, F_h is the total measured force in actuator, N is the vertical load on the isolator, R_{eff} is the effective radius of the isolator, u is the displacement at time t. Therefore, the coefficient of friction is determined by:

$$\mu(t) = \frac{F_\mu}{N(t)} \tag{5-2}$$

This approach can be used to determine the coefficient of friction if the relevant time-displacement-force data in digital format is available. An application about this approach can be found in (Gandelli, 2017). However, without having digitized data, it is extremely unlikely to interpret the hysteresis graphs correctly, especially at motion reversals (Constantinou et al., 2015).

The second approach can be used, if the digitized time-displacement-force data is not available, as in the case of this study. The only parameters required are the Energy Dissipated per Cycle, EDC, peak displacement (amplitude) and the vertical load on the isolator. Then, friction coefficient in the relevant cycle can be determined from the Energy Dissipated per Cycle as follows:

$$\mu_{ic} = \frac{EDC_i}{2(D_{max} - D_{min}) \cdot N} \tag{5-3}$$

where μ_{ic} is the coefficient of friction at ith cycle, EDC_i is the Energy Dissipated at ith cycle, D_{max} and D_{min} are the positive and negative peak displacements at ith cycle and N is the axial (vertical) load. In a typical test, the peak displacements at positive and negative sides of a cycle are identical, that is, $|D_{max}| = |D_{min}| = D_{amp}$ and vertical force is constant. Therefore, the equation can be written as follows:

$$\mu_{ic} = \frac{EDC_i}{4 \cdot D_{amp} \cdot N} \tag{5-4}$$

where D_{amp} is the displacement amplitude of the test and other terms are already defined. Energy Dissipation per Cycle can be expressed by integrating the force-displacement hysteresis, at the relative cycle of the test, of CSS isolators.

$$EDC = \int F \cdot du \tag{5-5}$$

where F is the horizontal force and u is the horizontal displacement measured at the test.

An application on the second approach can be found in Quaglini et al. (2012). In this study, the second approach is adopted to determine the friction coefficient along with to calibrate parameters for the friction model.

5.1 Velocity effect parameter calibration

The experimental results on DCSS isolators used in the hospital structure were not sufficient to give a clear understanding on the relationship between the coefficient of friction and the sliding velocity. For each dynamic test, the average sliding velocity was about 27 cm/sec with a peak velocity of 44 cm/sec which can be thought as high velocity, though do not provide the necessary information on friction coefficient at low velocities. Nonetheless, over the years of experiments on sliding-type isolators with PTFE-steel interface, it is now a well-known finding that the exponential equation (2-40) applies for the relationship between the friction coefficient and the sliding velocity. Moreover, taking the ratio of friction coefficient at low and high velocities, $\frac{\mu_{low}}{\mu_{high}}$, approximate, rather than exact does not considerably affect the peak displacement response of the CSS isolators, except for very low instesity of shaking, which is of no practical importance (Kumar et al., 2015). This may be attributed to the following reason. The friction coefficient tends to be remain unaffected by velocity once a threshold velocity is reached whereas the heating effect on the friction coefficient much more dependent on the duration of motion. In a typical seismic application, 50 cm/sec or larger sliding velocities are attained (Constantinou et al., 2007). Consequently, once the slider reaches typical velocities that occur during the course of seismic event, the friction coefficient will become insensitive to velocity effect thereafter. For the reasons explained, the parameters for velocity effect are $\frac{\mu_{low}}{\mu_{high}} = 0.5$ and $\alpha = 100\ \mathrm{sec/m}$ are used in this study.

5.2 Pressure effect parameter calibration

The parameters for pressure effect are calibrated using the results of displacement controlled, uni-directional sinusoidal tests conducted on specimens of the DCSS isolators used in hospital structure, as explained previously. Results of twenty-two tests covering a range of 9.5 to 45.7 MPa apparent contact pressures are utilized. It is required for friction model to obtain a pressure-friction relationship independent of that as a result of heating effect. This can be achieved using only the energy dissipation measured at the first cycle of movement for the calculation of friction coefficient, given that the heating effects are relatively small within the first cycle of movement (Trovato, 2013; Quaglini et al., 2012; McVitty and Constantinou, 2015; Gandelli, 2017). However, calibrating the pressure parameters using the test results of first-cycle friction caused the combined friction model to underpredict the friction coefficient in the test simulations that will be shown in further of this section. Thus, the influence of heating on the friction coefficient needs to be eliminated within the first cycle. For this purpose, the friction coefficients obtained from first-cycle of the tests are divided by the ratio of the second cycle value of the friction coefficient to the first cycle value (i.e., $\mu_{2c,test}/\mu_{1c,test}$). Taking an average of fifty-three high velocity tests performed under a range of 28 to 46 MPa, with slider diameters 255 to 505 mm, and displacement amplitudes 11.3 to 45 cm gives that the ratio $\mu_{2c,test}/\mu_{1c,test}$ is 0.83, which also means a reduction of 17% in the friction coefficient occurs in the first cycle.

Figure 5-1 shows results used for the calibration of the pressure parameters.Values of $c_1 = 3.14$, $c_2 = 0.293$, $c_3 = 0.043\ \text{MPa}^{-1}$,$c_4 = 0.227$ for $\mu_{ref} = 0.054$ and $p_{ref} = 39.1$ MPa are determined by employing a least square procedure. Therefore, the following equation represents the relationship between apparent pressure and the instanteneous friction coefficient

$$\mu(p) = \mu_{ref}\left(3.14(0.293^{0.043p} + 0.227)\right) \quad (5\text{-}6)$$

where all terms were defined previously. This equation is used in response history analyses to predict the instantenous effect of pressure on the friction coefficient.

To obtain a prediction for the first-cycle friction coefficient, equation (5-6) is modified by including the heating effect factor, $\mu_{2c,test}/\mu_{1c,test}$, as follows:

$$\mu_{1c}(p) = (\mu_{2c,test}/\mu_{1c,test})[\mu_{ref}(3.14(0.293^{0.043p} + 0.227))] \quad (5\text{-}7)$$

where μ_{1c} is the average first-cycle of friction coefficient predicted by the model, $\mu_{2c,test}, \mu_{1c,test}$ are the second and first cycle values obtained from tests respectively, and other terms were defined previously. The ratio $\mu_{2c,test}/\mu_{1c,test} = 0.83$ is used based on test results as mentioned previously.

Figure 5-1 shows the test results (see Table 5-1) on the apparent pressure and the first-cycle friction coefficient along with those predicted by the model using equation (5-7).

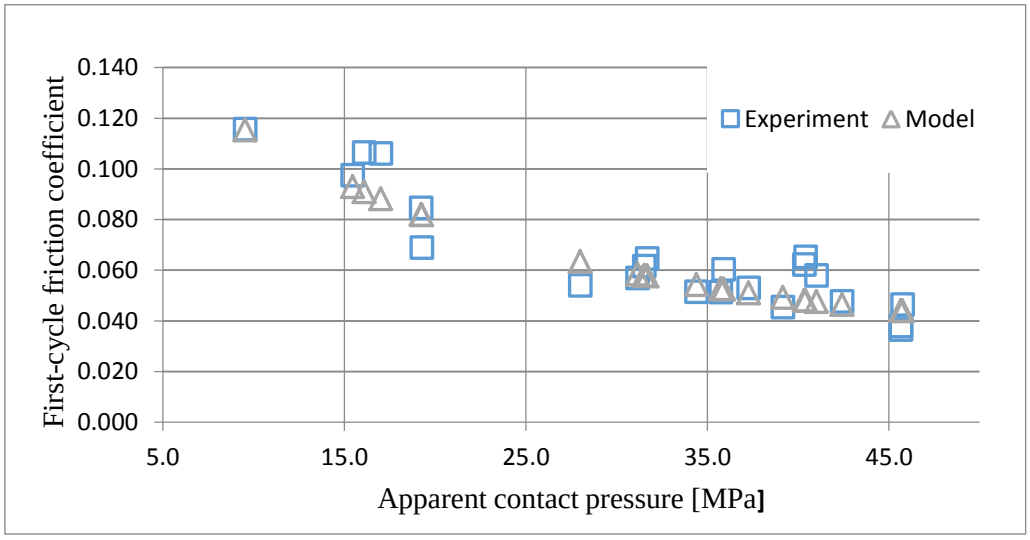

Figure 5-1. The relationship between apparent pressure and first-cycle friction coefficient according to test results and friction model used in this study.

After calibrating the heating parameters as will be shown in further in this chapter, the uni-directional tests are simulated through OpenSees to obtain the ratio of the three-cycle average friction to the first-cycle value are obtained. The results of the simulated tests give a value of 0.86 for the ratio of three-cycle average friction to

the first-cycle value. This also means that the friction coefficient inthe first cycle is 1.16 times the nominal friction coefficient (i.e. 1/0.86 =1.16), which reasonably close to a value of 1.20 proposed by other studies (Constantinou et al., 2011). That is,

$$\mu_{nom} = 0.86\mu_{1c} \tag{5-8}$$

where all terms defined previously.

Therefore, combining equations (5-7) and (5-6), an expression for the apparent pressure-nominal friction coefficient relationship is obtained as follows:

$$\mu_{nom}(p) = f_{h,nom}\left(\mu_{ref}\left(3.14(0.293^{0.043p} + 0.227)\right)\right) \tag{5-9}$$

where $f_{h,nom}$ is the adjustment factor to include the heating effect in the pressure model and other terms were defined previously. The factor, $f_{h,nom}$ is calculated by multiplying the ratio of second-cycle friction to first cycle (0.83) with the ratio of three-cycle average friction to first-cycle (0.86). Therefore,

$$\mu_{nom}(p) = (0.71)\left(\mu_{ref}\left(3.14(0.293^{0.043p} + 0.227)\right)\right) \tag{5-10}$$

where $\mu_{ref} = 0.054$ and other terms all terms were defined previously.

Table 5-1. Test results used for the calibration of the pressure effect parameters.

Tag	Amplitude [cm]	Average velocity [cm/sec]	Slider radius [mm]	Vertical load [kN]	Apparent pressure [MPa]	Energy Dissipation at first cycle [kNm]	Average friction coefficient at first cycle, μ_{1c}
1	45.0	27.0	128	1430	28.0	139.0	0.054
2	45.0	27.0	128	487	9.5	101.4	0.116
3	45.0	27.0	128	1610	31.5	178.8	0.062
4	26.5	27.0	128	1618	31.7	111	0.065
5	45.0	27.0	157.5	1498	19.2	228.2	0.085
6	45.0	27.0	157.5	3566	45.8	298.6	0.047
7	26.5	27.0	157.5	3559	45.7	138	0.037
8	45.0	27.0	157.5	1501	19.3	186.4	0.069
9	45.0	27.0	157.5	3559	45.7	243.4	0.038
10	45.0	27.0	157.5	3051	39.1	252.6	0.046
11	45.0	27.0	190	3533	31.2	362.5	0.057
12	45.0	27.0	190	1928	17.0	368.4	0.106
13	45.0	27.0	190	4071	35.9	442.5	0.060
14	26.5	27.0	190	4053	35.7	221	0.051
15	45.0	27.0	220	5667	37.3	540.6	0.053
16	45.0	27.0	220	2446	16.1	469	0.107
17	45.0	27.0	220	6235	41.0	650.9	0.058
18	26.5	27.0	220	6449	42.4	326	0.048
19	45.0	27.0	253	6888	34.4	644.7	0.052
20	45.0	27.0	253	3096	15.5	543.5	0.098
21	45.0	27.0	253	8094	40.4	951.4	0.065
22	26.5	27.0	253	8080	40.3	533	0.062

5.3 Heating parameter calibration

The parameters for heating effect on the coefficient of frictioncan be determined by means of temperature at the sliding interface. For this purpose, the temperature data is required. However, taking a direct temperature measurement through thermocouples out of sliding interface when the slider is in motion during a test is virtually impossible task (Constantinou et al., 2007). The thermocouple instruments can be embedded below the sliding surface but this gives the temperature on a few milimeter depth of actual sliding surface. Thermal imaging cameras might be of help to circumvent this issue by offering a non-contact means to measure the temperatures at the sliding interface (Trovato, 2013).

If the data on temperature at the sliding interface is not available, calibration of the heating effect parametrs can be treated as inverse problem as described in the following. The reduction in the friction coefficient due to frictional heating leads to decrease in energy dissipation, if the loading condition remains constant over the cycles, since the decrease in the friction coefficient results in decrease in lateral force response. Therefore, the energy dissipation for successive cycles in a cyclic test provides the information on decrease in the friction coefficient. A well-calibrated numerical model can simulate, reasonably close enough, the experimentally obtained force-displacement hysteresis and capture the decrease in energy dissipation between successive cycles. Thus, the heating effect parameters are sought by conducting a number of time history analyses, where the test conditions are simulated, with different heating effect parameters until the numerical and experimentally obtained force-displacement hystereses are reasonably close enough.

Since the data on the temperature at sliding interface is not available in this study, the aforementioned simulation approach is used to calibrate the heating parameters for the fricton model. An information on simulations is given in the folowing. The analyses are (1) displacement-controlled, (2) uni-directional, (3) sinusoidal displacement pattern with various frequencies, (4) constant vertical load. For

analysis, a CSS element with mechanical properties exactly same as corresponding test specimen is defined. An initial guess for the heating parameters are made. The constant vertical load is exerted on free end of the CSS model. Then, a predefined uni-directional, sinusoidal displacement pattern with a frequency that used in corresponding test is imposed to free end. A single point constraint with a displacement series can be used in OpenSees for this purpose. The duration of time-history analysis is set equal to the time required to complete all cycles in the respective test. Then, the force-displacement hysteresis, the friction coefficient and the energy dissipation are obtanied from numerical model and compared with corresponding experimental data. If these numerical response quantites does not match with the experiment, the heating parameters are changed and the analysis is repeated.

Table 5-2 shows the properties of the uni-directional tests used to calibrate heating effect parameters. The tests contain average results of sixteen different tests. The apparent contact pressure in each test is 39.1 MPa and the average sliding velocity 27 cm/sec. Table 5-3 and Table 5-4 presents energy dissipation and friction coefficient within successive cycles, respectively, obtained from tests and numerical model with the following heating parameters:

$$b = 0.60, \qquad c = 30\ (1/C°), \qquad d = 0.35, \qquad \phi = 0.942$$

Figure 5-2 illustures lateral force-displacement hysteresis obtained from test and numerical model for the uni-directional sinusiodal test with displacement amplitude 45 cm, which labeled as test 4. The peak resisting forces in the first cycle that occurs at the peak displacement $d_{max} = 45\ cm$ are 390 kN 380 kN for experimental and numerical model respectively. The numerical model estimates the friction coefficient in the first cycle with less than 5% error (0.043 and 0.045). Also, the model captures that the decrease in the friction coefficient from first cycle to second of 17%, and from first to third cycle of 23%, which reasonably close to those observed in test which are %19 and 28% respectively. The discrepancy in the friction coefficient between two test and numerical model is more pronounced at

low amplitude tests 2 and 3. The numerical model cannot capture the breakaway effects that occurs at motion reversals that can be barely seen in experimental data. On the other hand, there are good agreement between the numerical model and the experimental data in terms of overall force-displacement behavior.A smooth decrease in the resisting force with decrease in the friction coefficient can be seen from test data shown in part (a). On the other hand, an abrupt decrease in the resisting force can be observed on numerical model shown in part (b). This phenomenon is especially pronounced at lower values of displacement where slider close to the center of concave sliding surface. The reason for this behavior is explained in the following. The numerical model uses only the center of sliding interface to track the temperature information instead of several locations distributed across the surface, as described previously. At any given time in analysis, if the slider passes over center of sliding interface, the heat flux is generated at that point and the temperature rises. This occurs when the slider displacement is lower than the radius of slider, as it would indicate that the monitoring point falls within the area enclosed by the slider. As seen in part (b) of the figure, the abrupt changes in force-displacement hysteresis occurs at displacements of about ± 15 cm which almost equal to the slider radius (15.75 cm).

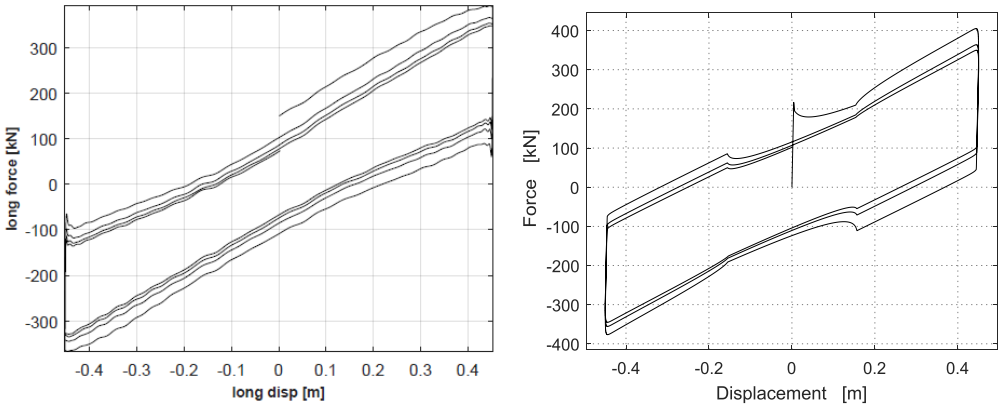

(a) (b)

Figure 5-2. Force-displacement hysteresis for test 4 with displacement amplitude 45 cm under 39.1 MPa, obtained from (a) prototype test, (b) numerical model

Table 5-2. Properties of the uni-directional sinusoidal tests.

Test tag	Displacement amplitude [cm]	Average velocity [cm/sec]	Slider radius [mm]	Vertical load [kN]	Apparent pressure [MPa]
1	11.3	27.0	157.5	3051	39.1
2	22.5	27.0	157.5	3051	39.1
3	33.8	27.0	157.5	3051	39.1
4	45.0	27.0	157.5	3051	39.1

Table 5-3. Energy dissipation under 39.1 MPa apparent pressure.

	Energy dissipation [kNm]							
	Test				Numerical			
Test tag	cycle 1	cycle 2	cycle 3	total	cycle 1	cycle 2	cycle 3	total
1	64	50	44	157	50	41	38	129
2	120	100	89	310	106	86	79	271
3	187	151	132	469	171	140	129	440
4	247	201	179	627	237	197	182	616

Table 5-4. Friction coefficients under 39.1 MPa apparent pressure.

	Friction coefficient							
	Test				Numerical			
Test tag	cycle 1	cycle 2	cycle 3	Avg	cycle 1	cycle 2	cycle 3	Avg
1	0.046	0.036	0.032	0.038	0.036	0.030	0.028	0.031
2	0.044	0.036	0.033	0.038	0.039	0.031	0.029	0.033
3	0.045	0.037	0.032	0.038	0.041	0.034	0.031	0.036
4	0.045	0.037	0.033	0.038	0.043	0.036	0.033	0.037

5.4 Combined effects and the friction model used in this study

Table 5-5: Summary of calibrated parameters of friction model.

Parameter	Value (unit)	Related effect
μ_{ref}	0.054	-
p_{ref}	39.1 (MPa)	Pressure
T_{ref}	20 (°C)	Heating
μ_{low}/μ_{high}	0.5	Velocity
α	100 (sec/m)	Velocity
c_1	3.14	Pressure
c_2	0.293	Pressure
c_3	0.043 (1/MPa)	Pressure
c_4	0.227	Pressure
b	0.60	Heating
c	30 (1/°C)	Heating
d	0.35	Heating
ϕ	0.942	Heating

Therefore, the following equations are used to determine instanteneous friction coefficient in the CSS isolators used in this study:

$$\mu(v, p, T) = \mu_{ref} k_v(v) k_p(p) k_T(T) \tag{5-11}$$

$$k_v(v) = 1 - 0.5\exp(-100|v|) \tag{5-12}$$

$$k_p(p) = 3.14(0.293^{0.043p} + 0.227) \tag{5-13}$$

$$k_T(T) = 0.942\left(0.60^{\frac{T}{30}} + 0.35\right) \tag{5-14}$$

where all terms are already defined.

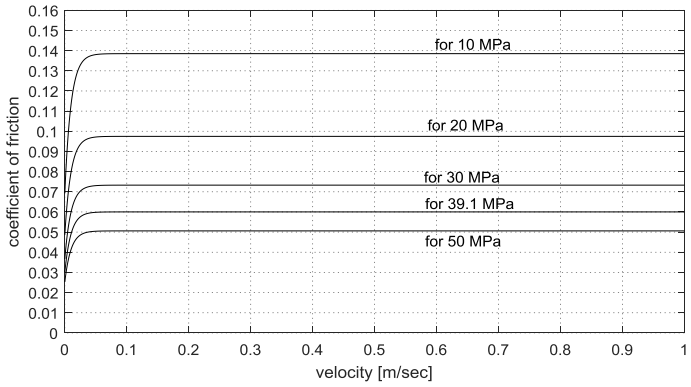

(a)

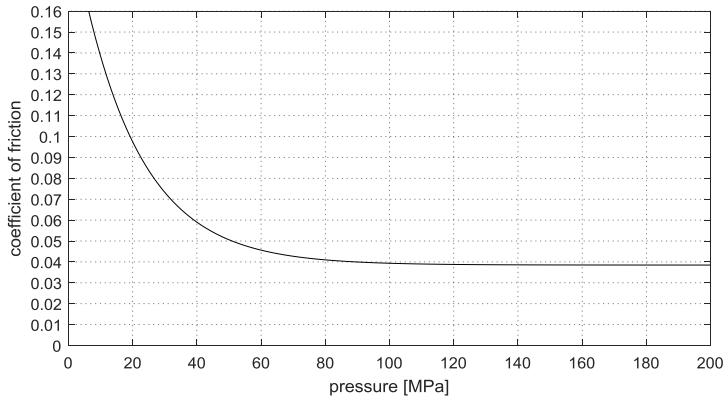

(b)

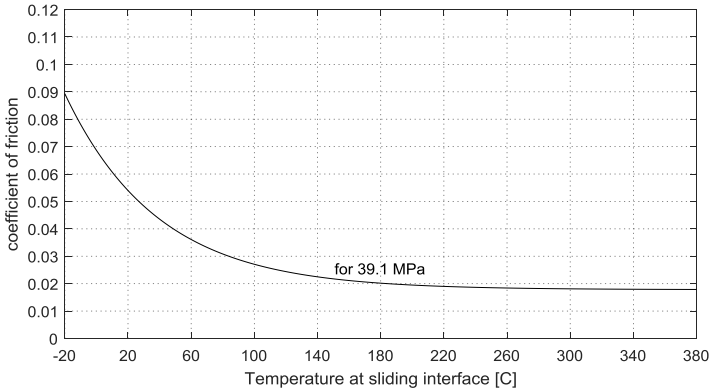

(c)

Figure 5-3. Relationship of friction coefficient with (a) sliding velocity, (b) apparent pressure, (c) temperature at sliding interface

CHAPTER 6

PROPOSED METHODS FOR CALCULATION OF SLIDER RADIUS

In practice of buildings isolated with CSS isolators, a target friction coefficient that the isolation sytem will operate is aimed. To this end, the dimensions of the isolators are designed so that average the entire isolators in the system is equal to the target friction. As discussed earlier, isolators are expected to perform under a wide range of axial loads. Considering the influence of the pressure on the friction coefficient, significant deviations from the target friction coefficient is expected for an individual isolator in the system. In theory, the dimensions of each isolator in the system can be altered to achieve the target friction coefficient to minimize the variations. However, this is extremely unlikely due to economical considerations associated to manufacturing. A common practice in design of large structures is to divide CSS isolators into groups according to their static axial loads so that the isolators with similar axial loads will be in the same group (Sarkistan et al., 2012). The major goal with this approach is to design a unique slider area for each group so that the friction coefficients of the isolators in the respective group will be close to each other, and also close to the target friction coefficient as much as possible. Typically, average of the axial loads on isolators (as a result of seismic weights) in each group is utilized to calculate the slider area for respective group to achieve the target friction coefficient. This method will be called as ‘Method 1’ in this study. Even if the isolators are seperated into groups in accordance with axial loads, the axial loads on isolators can differ significantly among individual isolators within the group, resulting in variations in the friction coefficient for isolators in that group. This will induce the eccentricity in the isolation system (Dicleli, 2020), and eventually may leads to torsion. In this study, two additional methods are proposed for the calculation of the slider area for each group of CSS isolators in the isolation system, to reduce the torsional response. ‘Method 1’ is the classical approach used

in design practice to estimate the slider area, and utilizes the arithmetic mean of the axial loads in the group. 'Method 2' introduces an iterative approach to estimate the slider area and utilizes the weighted mean of the friction coefficients of the isolators in a group. 'Method 3' utilizes equilibrium of the torsional moments produced by (1) the friction forces calculated using the Coulomb friction model and (2) the friction forces calculated using the friction model that calibrated for pressure effect.

In this study, the nominal friction coefficient is related to the apparent pressure through equation (5-10) as follows:

$$\mu_{nom}(p) = \left(f_{h,nom}\right)\left(\mu_{ref}\left(c_1\left(c_2^{c_3 p} + c_4\right)\right)\right) \tag{6-1}$$

where $p = N/A_{slider}$, being the apparent contact pressure; N, is the axial load, A_{slider}, is the slider area, μ_{ref}, is the reference coefficient of friction, c_1, c_2, c_3, c_4 are the calibration parameters for pressure effect obtained from experiments and $f_{h,nom}$ is the adjustment factor to include the heating effect in the nominal friction coefficient. Equation (6-1) is used to calculate the slider area that achieve the target friction coefficient. Thus, the equation should be solved for the slider area term to obtain open form solution. This might not be possible for the friction models in which the area term cannot be expressed explicitly. Substituting, $p = N/A_{slider}$ into equation (6-1) and after algabraic manipulations, the following equation for slider area,A_{slider}, can be obtained:

$$A_{slider} = \frac{N c_3 \ln(c_2)}{\ln\left(\frac{\mu_{target}}{f_{h,nom} c_1 \mu_{ref}} - c_4\right)} \tag{6-2}$$

where all terms are defined previosly.

6.1 Procedure to form groups

This section describes a procedure to divide isolators into groups based on axial loads. Definitions:

N_i: The static axial load on ith isolator in the system.

N_{min}, N_{max}: The minimum and maximum of the axial loads in the system.

m: The number of groups/types in the system, or equivalently, the number of different isolators to be manufactured.

ΔN: $(N_{max} - N_{min})/m$

First, the number of groups, m, is specified. Then, therange $[N_{min}\ N_{max}]$ is divided into m equally spaced intervals (groups). Thus, each group has bounds from $\big(N_{min} + (\Delta N)(k-1)\big)$ to $(N_{min} + (\Delta N)k)$ where k is the integer (from 1 to m) that represents the group tag. The ith isolator is assigned to group k, if the axial load of N_i falls within the interval of kth group.

6.2 Method 1: Arithmetic mean

Step 1: Specify the target coefficient of friction, μ_{target}.

Step 2: Calculate the arithmetic mean of static axial loads on isolators in the group. That is, sum up the axial loads on each isolator and divide the sum by the number of isolator in the group. This value is denoted by N_{avg}.

Step 3: Calculate the slider area, A_{slider}, to achieve μ_{target} by using equation (6-2).

6.3 Method 2: Iterative weighted mean

Step 1: Specify the target coefficient of friction,μ_{target}.

Step 2: Calculate the arithmetic mean of axial loads on isolators in the group. That is, sum up the axial forces on each isolator in the group and divide the sum by the number of isolator in the group. This value is denoted by N_{avg}.

Step 3: Calculate the initial slider area, $A_{slider,init}$ to achieve μ_{target} by using equation (6-2).

Step 4: Use the slider area, A_{slider}, with the individual axial load on each isolator to calculate friction coefficient, by using equation (6-1) for each isolator within the group. For the first iteration use the initial slider area,$A_{slider,init}$, for A_{slider}.

Step 5: Use the calculated friction coefficients as weight coefficients for the isolators to calculate the weighted mean of the axial load, N_{wavg}. That is, multiply the axial load on each isolator by the associated friction coefficient, sum up the results and divide by the summation of the friction coefficients for all the isolators within the group.

Step 6: Use the weighted mean of the axial load, N_{wavg}, calculated in previous step to calculate a new slider area, A_{slider}, to achieve μ_{target} by using (6-2).

Step 7: Repeat steps 4-6 until the results converge. That is, until the slider area calculated in the previous iteration is nearly equal to the one in the current iteration.

6.4 Method 3: Moment equilibrium

In the following,the equations pertaining to the calculation method 3 are necessary prior to explanatory steps. First, the friction force, $F_{f,i}$, acting on the isolator in the groupis expressed as follows:

$$F_{f,i} = \mu_i N_i \tag{6-3}$$

where μ_i is the friction coefficient, N_i is the axial load on the ith isolator in the group. Secondly, let select a reference point, O, which lies in the same plane with the isolation system. That is, O is a point onto the isolation system. Then, the moment, $M_{o,i}$, about the vertical axis passing through the point O, caused by the friction force acting on the ith isolator within the group is expressed as follows:

$$M_{o,i} = F_{f,i} d_i \tag{6-4}$$

where $F_{f,i}$ is the friction force acting on the ith isolator in the group, d_i is the distance between the ith isolator and the reference point O. Substituting (6-3) into (6-4), we obtain the following equation:

$$M_{o,i} = \mu_i N_i d_i \tag{6-5}$$

where all terms are already defined. Algabraic sum of the moments caused by friction forces within a group gives the torsional moment about the reference point for respective group. This summation is denoted by M_o which expressed as follows:

$$M_o = \sum_{i=1}^{n} M_{o,i} \tag{6-6}$$

where n is the number of isolators in the respective group and other terms are defined previosly.

The following steps are applied for each group in the isolation system:

Step 1: Specify the target coefficient of friction, μ_{target}. Select a reference point, O, which lies in the same plane with isolation system.

Step 2: Calculate the friction forces for the isolators in the group using equation (6-3), assuming the friction coefficients for the isolators are identical and equal to the target friction coefficient μ_{target}. That is, multiply the target friction coefficient by the axial load of the respective isolator in the group.

Step 3: Calculate the sum of the moments about the point O produced by the friction forces calculated at previos step, as shown in equations (6-4) and (6-6). Let this sum be M_{uni}.

Step 4: Find the slider area, A_{slider}, that results in the sum of the actual moments about the point O produced by the actual friction forces, which calculated through the actual friction coefficients (using equation (6-1)) within the group, is equal to M_{uni}.

It is useful provide further information on step 2 through 4. In steps 2 and 3, the sum of the moments about the refrence point is calculated as if the friction coefficient for all isolators in the group is identical to μ_{target}. This expression can be written as follows:

$$M_{uni} = \sum_{i=1}^{m} \mu_{target} N_i d_i \quad (6\text{-}7)$$

where M_{uni} is the sum of the moments, μ_{target} is the target friction coefficient, N_i is the axial load on ith isolator, d_i is the distance between reference point and ith isolator, m is the number of isolators in the group. Then, through step 4, a slider area,A_{slider},is soughtso that the following equation holds:

$$M_{uni} = \sum_{i=1}^{m} \mu_i N_i d_i \quad (6\text{-}8)$$

where μ_i is the actual friction coefficient which calculated using equation (6-1) and other terms are defined previously. A trial and error strategy or an optimization method, can be used to find the appropriate slider area that satisfies the equation (6-8), since the open form solution for slider area term cannot be obtained from this equation.

6.5 Implementation of the proposed methods

The implementation of the proposed methods for the calculation of the slider are presented herein. To this end, the isolators in 'Model A' is divided into three groups based on the axial loads. Then, the slider area for each group is determined for three methods described previously.

Axial loads on 234 CSS isolators are obtained through static analysis. Sorted axial loads are presented in Figure 6-1. The average, minimum and maximum loads are presented on Table 6-1. Apparent pressure-nominal friction coefficient relationship is set by calibrating the parameters related to the pressure effect, using the prototype test results as already mentioned in the preeceding sections. The calibrated parameters were $c_1 = 3.14, c_2 = 0.293, c_3 = 0.043 \frac{1}{\text{MPa}}, c_4 = 0.227$, along with reference parameters $p_{ref} = 39.1$ MPa, $\mu_{ref} = 0.054$ and the adjustment factor for the heating effect $f_{h,nom} = 0.71$.

Table 6-1. Static axial loads on the isolators for 'Model A'.

		Axial load [kN] (Compressive)		
Group no	# isolators	Mean	Min	Max
1	121	2646	1537	3340
2	66	4223	3428	5180
3	47	6083	5229	7058
All	234	3781	1537	7058

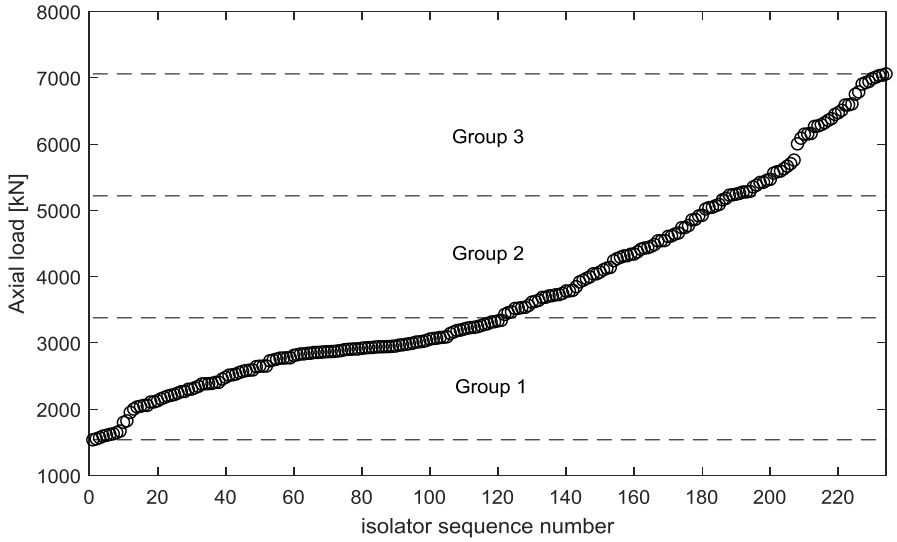

Figure 6-1. Static axial loads on the isolators in ascending order for 'Model A'.

The calculations have been made for the group 1 are given as follows:

Method 1: Arithmetic mean

Step 1: Specify target friction coefficient.$\mu_{\text{target}} = 0.05$.

Step 2: Arithmetic mean of the static axial loads on the isolators within the group is read from Table 6-1, $\text{N}_{\text{avg}} = 2646$ kN.

Step 3: The slider area to achieve μ_{target} is calculated by using equation (6-2). Here, the calibrated parameters for the pressure efffect are substituted into the equation (6-2) as well as N_{avg}. That is,

$$A_{slider} = \frac{(2.646\ \text{MN})(0.043)(1/\text{MPa})\ln(0.293)}{\ln\left(\frac{0.05}{(0.71)(3.14)(0.054)} - 0.227\right)}$$

$A_{slider} = 0.0837\ \text{m}^2$ or equivalently, $R_{slider} = 0.163$ m (163 mm).

Method 2: Iterative weighted mean

Step 1: Specify target friction coefficient.$\mu_{target} = 0.05$.

Step 2: Arithmetic mean of the static axial loads on the isolators within the group is read from Table 6-1. The value of $N_{avg} = 2646$ kN.

Step 3: Theinitial slider area, $A_{slider,init}$, to achieve $\mu_{target}$is calculated by using equation (6-2). Here, the calibrated parameters for pressure efffect are substituted into the equation (6-2) as well as N_{avg}.

$$A_{slider,init} = \frac{(2.646\ \text{MN})(0.043)(1/\text{MPa})\ln(0.293)}{\ln\left(\frac{0.05}{(0.71)(3.14)(0.054)} - 0.227\right)}$$

$A_{slider,init} = 0.0837\ \text{m}^2$

Step 4: Using the initial estimate for the slider area for the first iteration, along with the individual axial load on each isolator, the friction coefficient for each isolator in the group is calculated.

Step 5: The calculated friction coeffficients are used as weight coefficients for the isolators to calculate weighted mean of the axial load, N_{wavg}. The calculated value is $N_{wavg} = 2574$ kN.

Step 6: By using (6-2) with calculated N_{wavg}, a new slider area, A, is calculated as follows:

$$A_{slider} = \frac{(2.574\ \text{MN})(0.039)(1/\text{MPa})\ln(0.408)}{\ln\left(\frac{0.05}{(3.25)(0.043)} - 0.122\right)}$$

$A_{slider} = 0.0814\ \text{m}^2$. (Result for first iteration)

Step 7: Steps 4 through 6 is repeated until the slider area converge.

After 2 iteration, the slider area has converged to $A_{slider} = 0.0814\ m^2$, or equivalently, $R_{slider} = 0.161\ m\ (161\ mm)$. The results are presented on Table 6-2.

Table 6-2: Results of the implementation of the Method 2 for Model A3.

Group no	Calculated slider radius	Weighted mean axial load	Apparent contact pressure
-	R_{slider} [mm]	N_{wavg}[kN]	N_{wavg}/A_{slider} [MPa]
1	161	2574	32
2	205	4177	32
3	246	6035	32

Method 3: Moment equilibrium

Step 1: Specify target friction coefficient.$\mu_{target} = 0.05$. A reference point, O, on the isolation system is arbitrarly selected.

Step 2: The friction forces for the isolators in the group are calculated, assuming the friction coefficients for the isolators are identical and equal to that of target, or, $\mu = 0.05$.

Step 3: Sum of the moments about the reference point, O, produced by the friction forces calculated in the previous step, is determined as follows:$M_{uni} = 750828\ kNm$.

Step 4: A value of $R_{slider} = 163$ mm is used as initial guess for the radius of slider. Corresponding moment is calculated as $M = 760040\ kNm$, which gives M/M_{uni}=1.02. After a few trials, $R_{slider} = 161mm$ is found (M/M_{uni}=1.00).

6.6 Summary of isolation system under consideration

The radius of slider of each group used within isolation systems that will be analyzed are presented on Table 6-3 through Table 6-5. The isolators with corresponding group tag can be seen from Figure 6-2 through Figure 6-4.

Table 6-3. Radius of slider for groups for 'Model A'.

group label	Radius of slider [mm]		
	Slider area calculation method		
	1	2	3
Number of groups = 1			
1	195	186	189
Number of groups = 2			
1	171	168	169
2	236	234	234
Number of groups = 3			
1	163	161	161
2	206	205	206
3	247	246	248
Number of groups = 5			
1	147	145	147
2	176	176	176
3	207	207	207
4	231	231	230
5	257	257	256

Table 6-4. Radius of slider for groups for ‘Model B’.

group label	Radius of slider [mm]		
	Slider area calculation method		
	1	2	3
Number of groups = 1			
1	212	195	203
Number of groups = 2			
1	212	180	182
2	310	307	308
Number of groups = 3			
1	176	171	172
2	257	254	258
3	328	327	326
Number of groups = 5			
1	166	163	163
2	218	216	214
3	261	260	261
4	301	301	300
5	342	341	341

Table 6-5. Radius of slider for groups for ‘Model C’.

group label	Radius of slider [mm]		
	Slider area calculation method		
	1	2	3
Number of groups = 1			
1	205	193	206
Number of groups = 2			
1	194	186	192
2	297	294	299
Number of groups = 3			
1	181	176	178
2	251	249	253
3	321	319	321
Number of groups = 5			
1	170	167	168
2	219	217	218
3	260	259	260
4	301	301	301
5	342	342	341

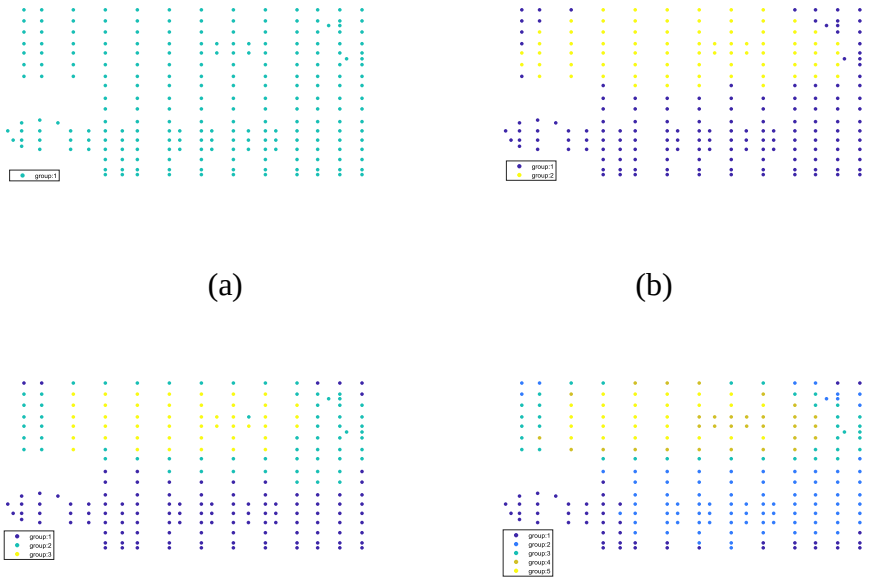

(a) (b)

(c) (d)

Figure 6-2: Isolation system layout of ‘Model A’ for number of groups is equal to (a) 1, (b) 2, (c) 3, (d) 5.

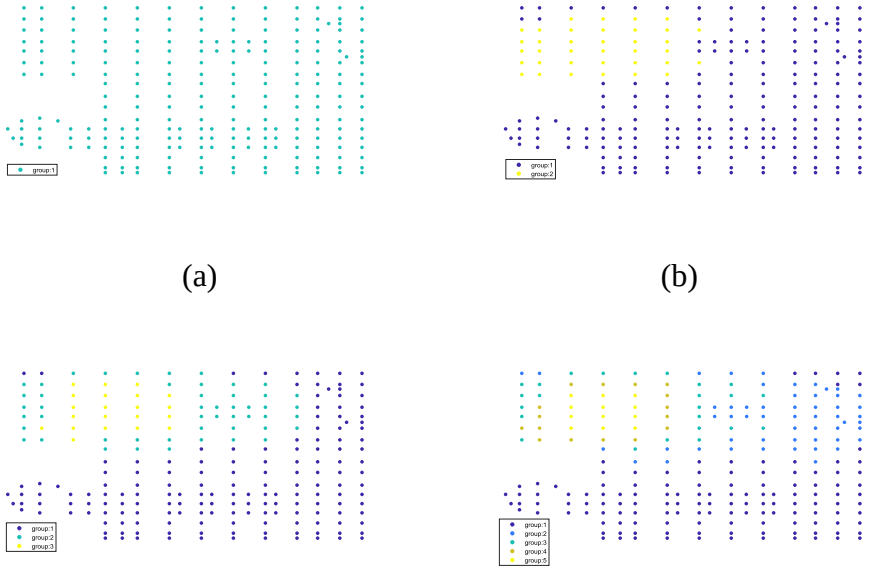

(a) (b)

(c) (d)

Figure 6-3. Isolation system layout of ‘Model B’ for number of groups is equal to (a) 1, (b) 2, (c) 3, (d) 5.

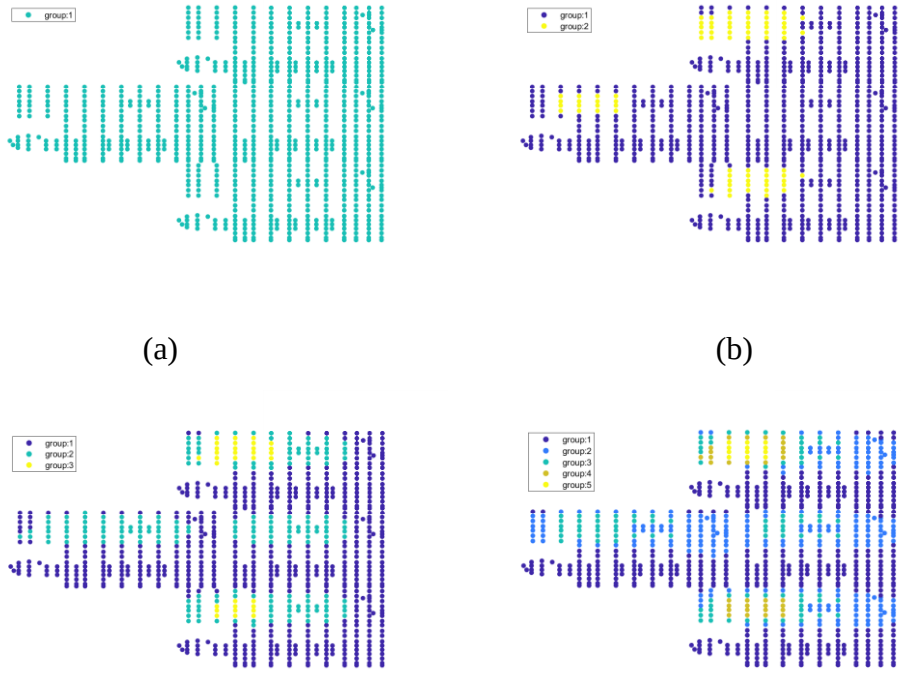

(a) (b)

(c) (d)

Figure 6-4. Isolation system layout of ‘Model C’ used in this study for number of groups is equal to (a) 1, (b) 2, (c) 3, (d) 5.

CHAPTER 7

NONLINEAR RESPONSE HISTORY ANALYSES

A number of nonlinear response history analyses (NLRHA) were conducted in OpenSees.The focus of the analyses are classified in two groups: (1) effect of the friction model on response of individual isolators, (2) parameters that influence the torsional response of the isolation system.

7.1 Effect of friction model on response of individual isolators

The effect of friction model on response of the isolators are discussed using 'Model A' with number of groups is equal to 1. For this purpose, Kobe 1995 (GM 1) record with scale factor 1.54 was used. The analyses were performed for 25 seconds. Newmark beta integrator with 'ModifiedNewton' algorithm were used. The integration time step was set equal to 0.01 seconds initially, and down to 10^{-8}seconds was allowed in case of converge problems. Time steps lower than 0.01 seconds were tried, and found that the results obtained with lower time steps are identical to those obtained with 0.01 seconds. The stiffness proportional damping of 2% of critical damping was assigned to structure, given that the superstructures perform within their elastic limit, while 'FPBearingPTV' elements were assigned zero viscous damping. The columns ands beams were modeled with 'elasticBeamColumn' frame element, the shear walls were modeled with 'ShellDKGQ' element.'rigidDiaphragm' constraints were used to model diaphragm in floor slabs. In analyses where Coulomb friction model used, the friction coefficient of 0.05 were assigned to isolators. The parameters under consideration are presented on Table 7-2.

Table 7-1. Friction models used in the response history analyses.

Friction dependency	Symbol
Coulomb (constant)	-
Pressure	P
Velocity + Pressure	V+P
Velocity + Heating	V+H
Pressure + Heating	P+H
Velocity + Pressure + Heating	V+P+H

Table 7-2. Parameters under consideration in the response history analyses.

Analysis no	Friction dependency				GM excitation	Isolator location	Plot
	Coulomb	Velocity	Pressure	Heating			
1	x	-	-	-	Bi-lateral	center of rigidity	Figure 7-1, Figure 7-2, Figure 7-3
2	-	-	x	-	Bi-lateral	center of rigidity	Figure 7-2, Figure 7-3
3	-	x	x	-	Bi-lateral	center of rigidity	Figure 7-2, Figure 7-3
4	-	x	-	x	Bi-lateral	center of rigidity	Figure 7-2, Figure 7-3
5	-	-	x	x	Bi-lateral	center of rigidity	Figure 7-2, Figure 7-3
6	-	x	x	x	Bi-lateral	center of rigidity	Figure 7-1, Figure 7-2, Figure 7-3, Figure 7-4
7	-	x	x	x	Tri-dir	center of rigidity	Figure 7-4, Figure 7-5
8	-	x	x	x	Tri-dir	corner 2	Figure 7-5

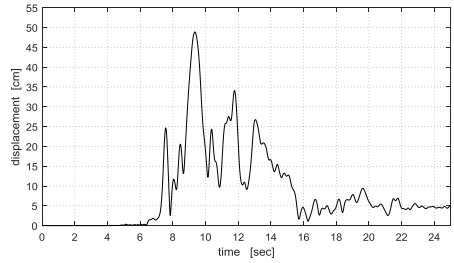

(a) Resultant disp. for Coulomb

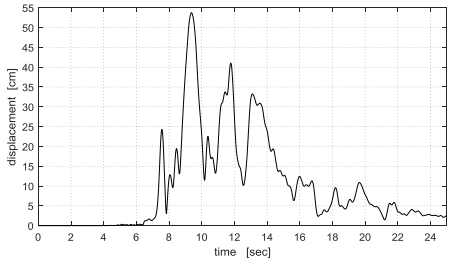

(b) Resultant disp. for (V+P+H)

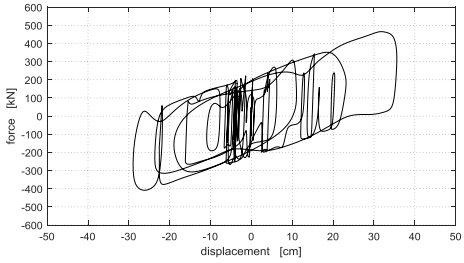

(c) Hysteresis for Coulomb

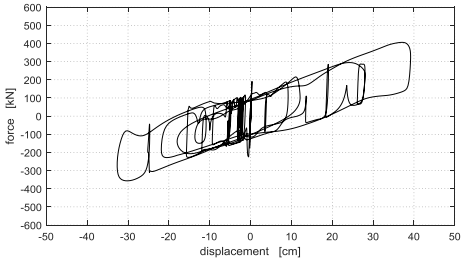

(d) Hysteresis for (V+P+H)

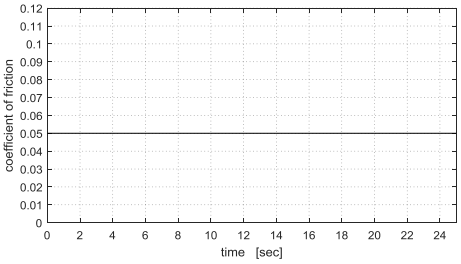

(e) Friction coeff. for Coulomb

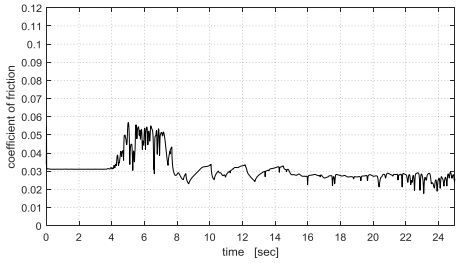

(f) Friction coeff. for (V+P+H)

Figure 7-1. Response histories of the isolator located at the center of rigidity for two friction models.

Difference between Coulomb and (V+P+H) dependent friction models is evident from Figure 7-1. As shown in parts (a) and (b), peak resultant displacement displacements are 49 and 54 cm for Coulomb and (V+P+H) respectively, indicates an underestimation by an amount of 10% by Coulomb friction model. Although it is not presented here, the difference is more pronounced at corner isolators where the peak displacements are underestimated by 15%. Moreover, due to degradation of friction coefficient, the area enclosed by force-displacement hysteresis tends to

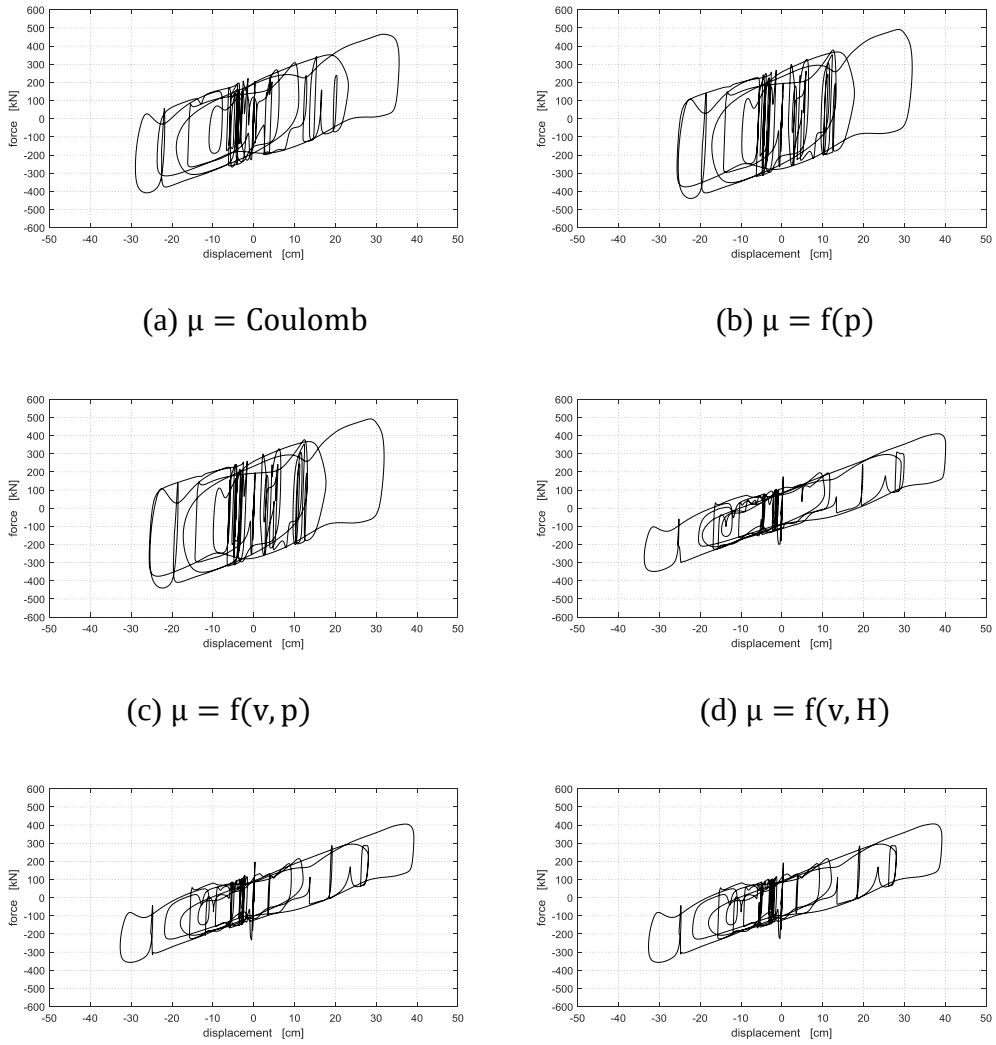

(a) μ = Coulomb

(b) $\mu = f(p)$

(c) $\mu = f(v, p)$

(d) $\mu = f(v, H)$

(e) $\mu = f(p, H)$

(f) $\mu = f(v, p, H)$

Figure 7-2. Displacement-force hysteresis of the isolator located atthe center of rigidity, subjected to GM 1 bi-lateral,for different friction models.

shrink in (V+P+H) model as shown in part (d), while Coulomb model cannot capture this phenomenon. Finally, estimated friction coefficients are presented in parts (e) and (f).

Figure 7-2 shows force-displacement hysteresis for all friction models. The width of the hysteresis along ordinate axis is proportional to $2\mu N$. Energy dissipation decreases as the width decreases.

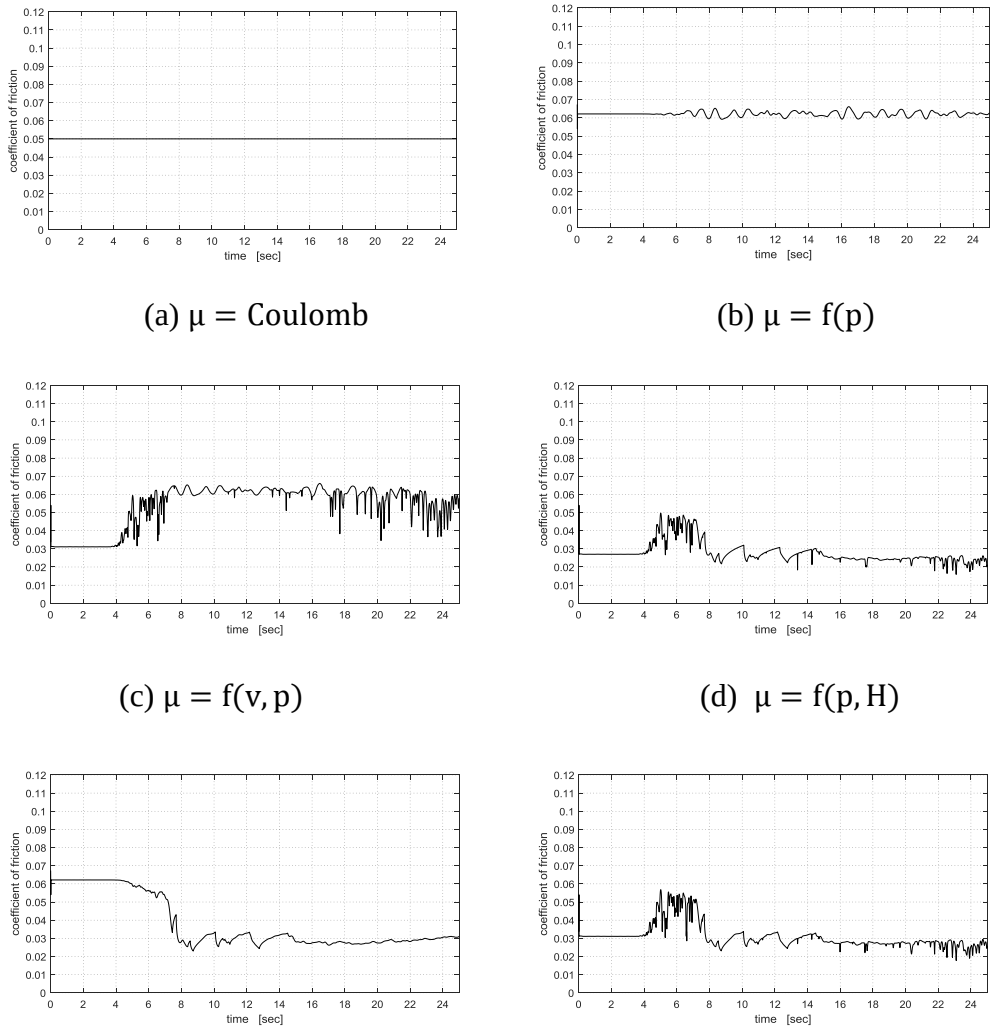

(a) $\mu = \text{Coulomb}$ (b) $\mu = f(p)$

(c) $\mu = f(v, p)$ (d) $\mu = f(p, H)$

(e) $\mu = f(p, H)$ (f) $\mu = f(v, p, H)$

Figure 7-3. Histories of coefficient of friction in the isolator located at the center of rigidity for different friction models.

The models that accounts for heating effect are able to capture the decrease in width of the hysteresis as shown in parts (d), (e) and (f), while other models overestimates the energy dissipation.

Figure 7-3 shows the history of friction coefficient in CR isolator for all friction models. The coefficient is constant and equal to 0.05 in Coulomb model as shown in part (a). Part (b) shows pressure dependent model. The coefficient slightly

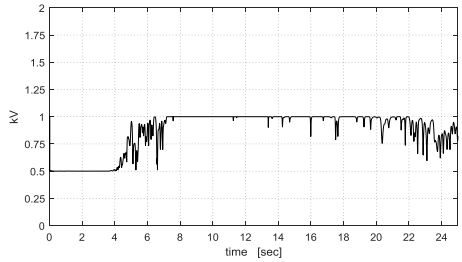

(a) Velocity fact., bi-lat. GM

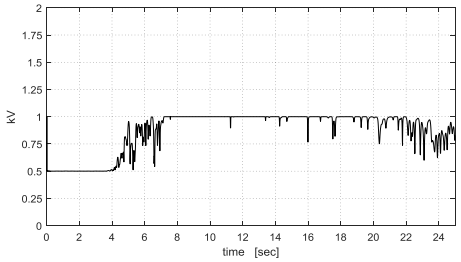

(b) Velocity fact., tri-dir. GM

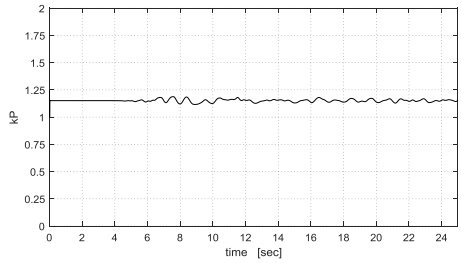

(c) Pressure fact., bi-lat. GM

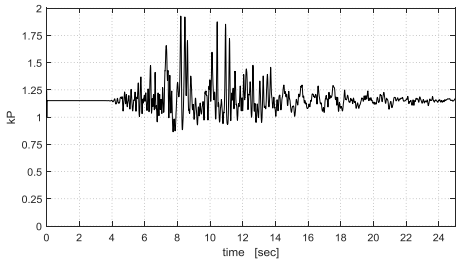

(d) Pressure fact., tri-dir. fact

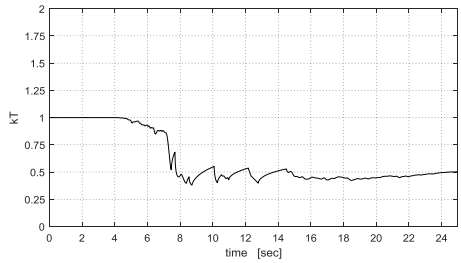

(e) Heating fact., bi-lat. GM

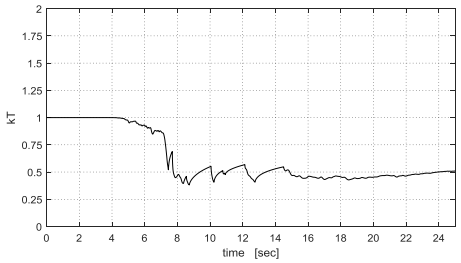

(f) Heating fact., tri-dir. fact

Figure 7-4. Histories of factors accounting for the influences of velocity, pressure, heating effect using $\mu=f(v,p,H)$ under two GM type.

oscillates around 0.062. Part (c) represents (V+P) dependent model. High frequency fluctuations are observed due to effect of velocity. The mean friction is equal to 0.059. Parts (d) and (e) shows (P+H) and (V+P+H) dependent models respectively. It is evident that friction coefficient tends to decrease due to heating. The mean friction coefficient observed is 0.031 for 5 to 25 seconds.

Figure 7-4 shows the histories of factors that accounts for velocity, pressure and heating effects on friction in CR isolator, estimated under bi-lateral and tri-directional excitations. Parts (a) and (b) shows the velocity factors for two type of

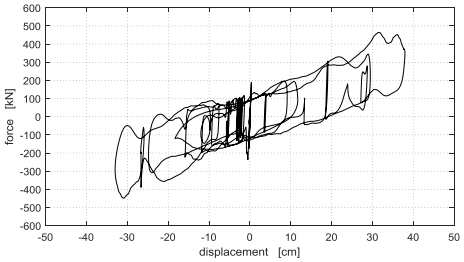

(a) Hysteresis at CR

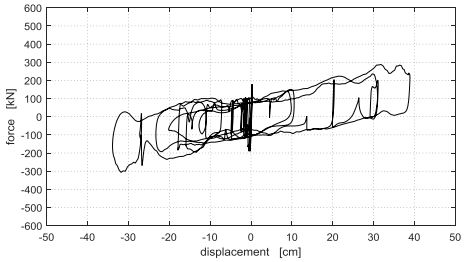

(b) Hysteresis at corner 2

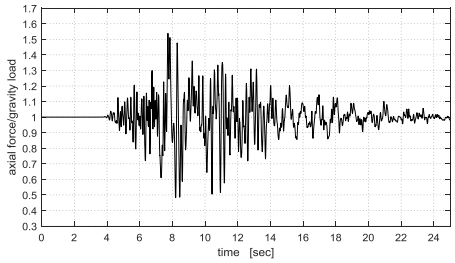

(c) Norm. axial force at CR

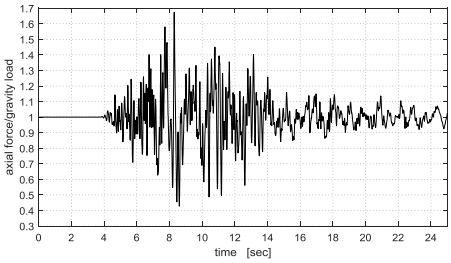

(d) Norm. axial force at corner 2

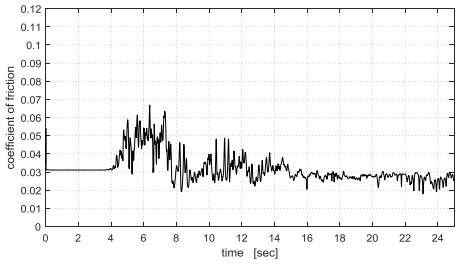

(e) Fric. coeff. at CR

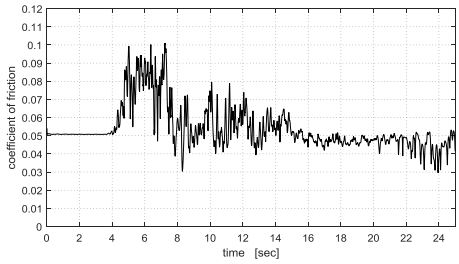

(f) Fric. coeff at corner 2

Figure 7-5. Response histories for isolators at center of rigidity (CR) and corner 2 for μ=f(v,p,H) under tri-dir GM.

excitations. The mean value is equal to 0.96 for both cases. A velocity factor close to unity indicates that isolator slides with a high velocity for most of times during the motion. Parts (c) and (d) shows histories of pressure factor. In bi-lateral excitation case, factor starts with a value of 1.25, which indicates the apparent pressure on the isolator tends to increase the friction by a factor of 1.25 at the very beginning of motion. Mean value of the pressure factor 1.15 and 1.17 for bi-lateral and tri-directional cases respectively. Thus, inclusion of vertical component of excitation have a minor effect on friction coefficient.

Response of two isolators located at CR and corner can be seen in Figure 7-5. Parts (a) and (b) shows force-displacement hystereses of these isolators. The isolator at CR has a more stiff response than that of corner isolator. This can be attributed to differences in axial loads on the isolators. CR isolator has a static axial load of about 4450 kN while the corner isolator under a 2240 kN. Higher axial force provides more higher post-yield (sliding) stiffness to CR isolator as seen in part (a). Furthermore, the axial loads on both isolators fluctuates severely due to presence of vertical component of the excitation, and due to overturning effects. The latter is more pronounced at the corner isolator, as can be seen in part (d), in which the axial load reachs as much as 1.68 times of what would experience under estatic load. On the other hand, CR isolator is moderately affected by axial load fluctuations. The effect of axial load is manifested most significantly on the friction coefficient, as shown in parts (e) and (f), since the apparent pressures acting on the isolators are different.

7.2 Torsional response of isolation system

7.2.1 Evaluation of torsional response

There are different approaches in literature to quantify the torsional response of an isolation system. Nagarajaiah et al. (1993) used the ratio of peak corner displacement to the peak displacement at center of mass to evaluate additional displacements due to torsion. They also used the ratio of dynamic torque to the static torque, of which the latter is defined as the SRSS of torques in principal directions that resulted from peak structural shear force obtained in dynamic analysis multiplied by the static eccentricity.

Wolff et al. (2014) introduced the torsional amplification ratio, D_C/D_{CR}, which is defined as the peak displacement at corner isolator (D_C) to the peak displacement at the center of rigidity of isolation system (D_{CR}).

Mazza (2017) used the floor rotation at the level of the isolation system as an indicator of torsion.

In this study, the approach given by Wolff et al. (2014) is used to evaluate the torsional response. The amplification ratio, D_C/D_{CR}, is used as an indicator of the extent of torsional response of the isolation system. Thus, D_C/D_{CR} is close to unity indicates the torsional response is small. The farther away from unity, the higher the torsional response of the system.

Extent of torsion-induced displacement is not same for each corner isolator. Torsion cause an increase at isolators located at 'flexible' edge/side of the isolation system, whereas it cause a decrease at displacements located at the 'stiff' edge/side. The terms 'flexible' and 'stiff edge of a structure represents the sides where under a static eccentric lateral force, the displacement due to pure torsion is added or subtracted, respectively, to the displacement at center of rigidity due translational response (Anognostopoulos et al., 2013). The additional displacement in corner isolators due to torsion is only concern from design perspective, as the displacement capacity of the isolators may need to be increased (Dicleli, 2020). For this reason,D_C/D_{CR} ratios that equal to or greater than 1.0 are of interest in this work.

For each model analyzed the isolators located at corners of the isolation system were monitored, and the relative displacements were recorded throughout the analysis. Furthermore, the isolator that closest to the center of rigidity was also monitored. The information on selection of these isolators have been given in Chapter 3. For each analysis, the square root sum of the squares (SRSS) at each time step was used to calculate the resultant displacement of the isolators, and peak resultant displacements were determined. The analyses were undertaken for seven ground motions mentioned in previous chapters. For each monitored isolator, the average of the seven peak resultant displacements was calculated. Then, the amplification ratio, D_C/D_{CR}, for each corner isolator was calculated by dividing the average peak displacement of respective corner isolator by the average peak

displacement of center of rigidity isolator. Finally, the value of ratio D_C/D_{CR} among corner isolators that yields worst result (i.e., highest D_C/D_{CR} ratio) was used as the torsional amplification ratio of the case under consideration.

7.2.2 Classification of investigated parameters

Influences of the several parameters on the torsional response of isolation system are investigated. These parameters are: (1) the friction model used in analysis, (2) the method for calculation of slider radius, (3) the number of groups within isolation system, (4) the ground excitation.

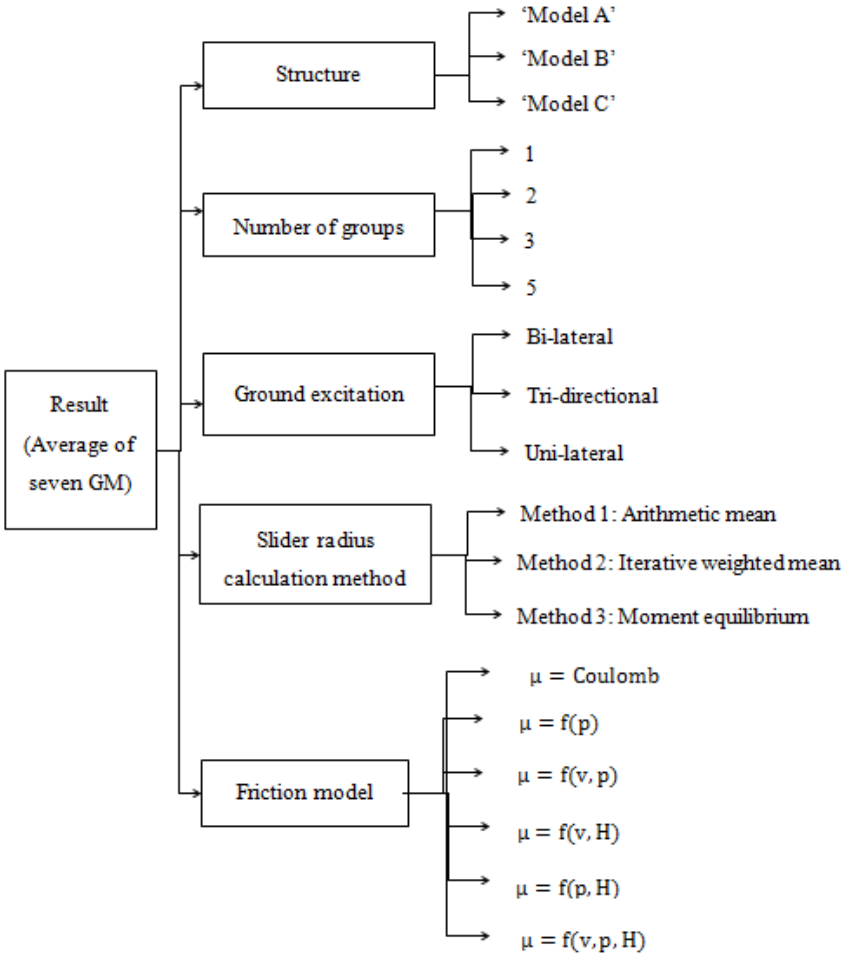

Figure 7-6. Diagram of the influence parameters investigated.

7.2.3 Effect of ground excitation

Torsional amplifications on the isolation system are identical for almost all friction models under bi-lateral and tri-directional excitations, indicating that the vertical component of the ground excitation has minor effect on torsional response.

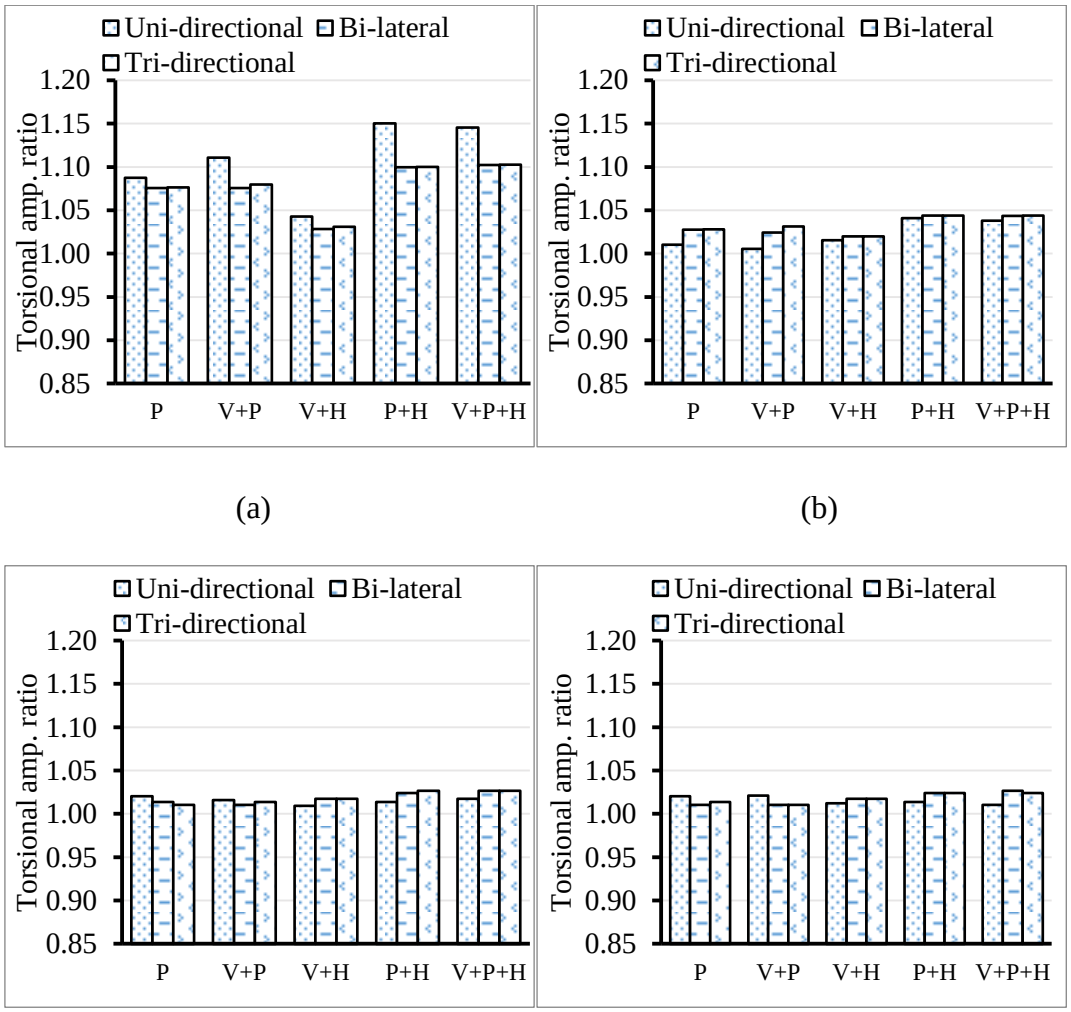

Figure 7-7: Torsional amplification ratio under uni-directional, bi-lateral, tri-directional excitations obtained using 'Model A' for (a) number of groups = 1, (b) number of groups = 2, (c) number of groups= 3, (d) number of groups = 5.

7.2.4 Effect of friction model

The analyses presented herein consider the case where structures with number of groups within isolation system is equal to one, and the slider calculation method is 'Method 1'. The analyses were conducted for tri-directional excitation. Figure 7-8 shows the torsional amplifacation ratios of the structures for five friction models.

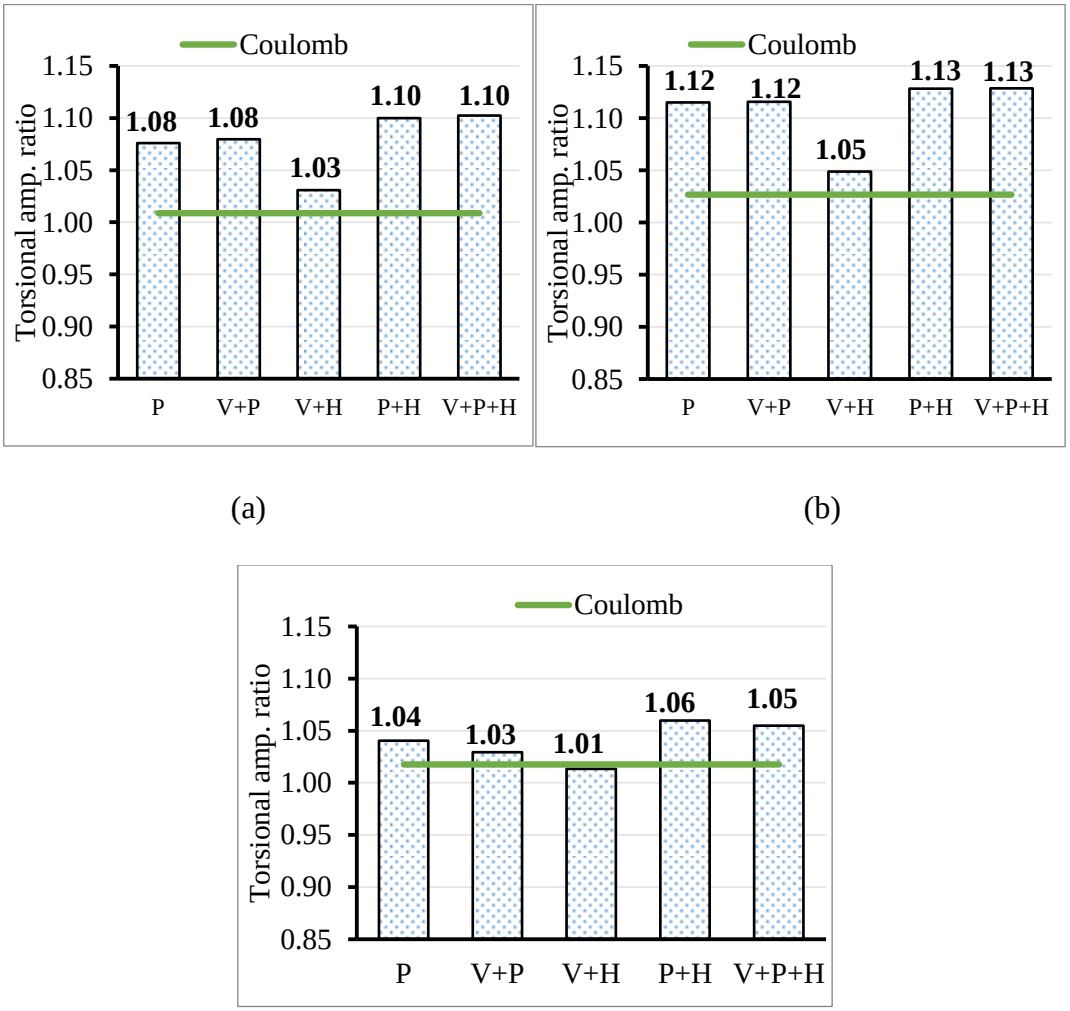

Figure 7-8. Torsional amplification ratios for friction models for (a) 'Model A', (b) 'Model B', (c) 'Model C'.

The results of Coulomb friction model, given as line plot, represent the reference case where torsion on the isolation system is independent of isolation system eccentricity which results from difference in friction among isolators. The friction model used in analysis has a major influence on the torsional response of the isolation system.

Although it has been shown in Chapter 5 that the Coulomb friction model does not apply for isolators under consideration, the analyses in which Coulomb friction is assumed still convey an information about the torsion on the isolation system that results from other factors such as superstructure eccentricity. Indeed, there are still a small amount of torsion on the isolation system for Coulomb friction cases, as can be seen from Figure 7-8, and it can be attributed to superstructure eccentiricty. The torsional amplification ratios obtained from corresponding Coulomb friction case are 1.01, 1.03 and 1.02 for 'Model A', 'Model B' and 'Model C' respectively.

The velocity dependency of friction seems to have little or no effect on torsional response on the isolation system.

The effect of pressure dependency of friction on torsional response of the isolation system is evident from the figure. The torsional amplification ratios for 'Model B' are 1.03 and 1.05 for Coulomb and (V+H) dependent friction cases respectively, as seen from part (b) of the figure, whereas a value of 1.13 can be observed when the pressure dependency is accounted for.

The effect of heating dependency on torsion is pronounced, though, it is not as strong as pressure effect.

7.2.5 Effect of number of groups and method

The effect of number of groups within isolation system and the effect of method used for calculation of slider radius on torsional response is investigated. For this purpose, the results of number of analyses are presented in this section. In analyses, velocity, pressure and heating dependent friction model was used in isolators and the structures were subjected to tri-directional excitation, as these conditions represents the most realistic situation.

Figure 7-9 shows the torsional amplification ratio against the number of groups for three methods used for calculation of slider radius for three structures. The difference in torsion on isolation systems among the three models is evident. This is because differences in structure parameters such as slenderness and static eccentricity. For example, 'Model B' had largest asymmetries in elevation, which makes it more susceptible to overturning effects, has the largest torsional amplification ratios.

It can be seen that the torsion on isolation system decreases as the number of groups increases. This can be attributed to the decrease in deviation of friction coefficients in isolators from the target friction. As more groups are formed and slider dimensions are altered for each group, the friction properties of the isolators will be close to each other, and thus the static eccentricity reduces.

The method used for calculation of slider has very limited effect on torsional response. Of 12 cases (4 groups x 3 models) presented herein, 'Method 2', which utilizes an iterative approach to estimate slider radius, provide a decrease in torsional amplifacation ratios by an amount of 1 percent for 5 cases, 2 percent for 1 cases over traditional 'Method 1', which is commonly used in practice, and both methods yield the same results for remaining 6 cases, as it can be seen from the figure. Similar observations can be made for 'Method 3'.

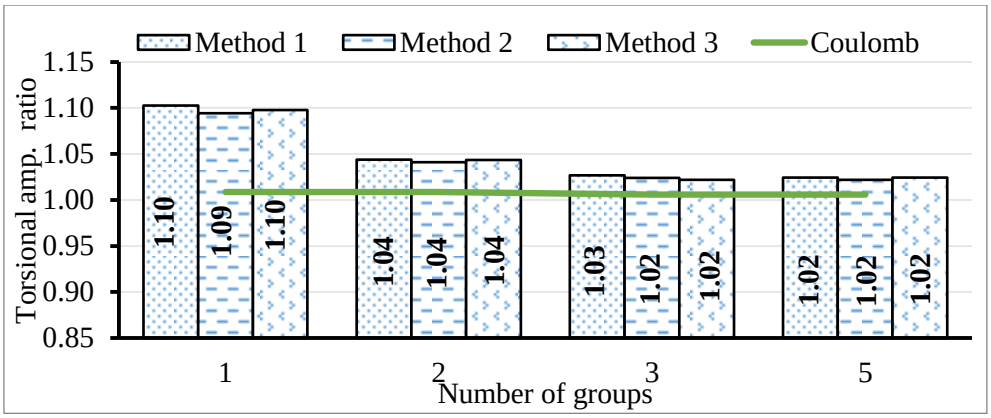

(a)

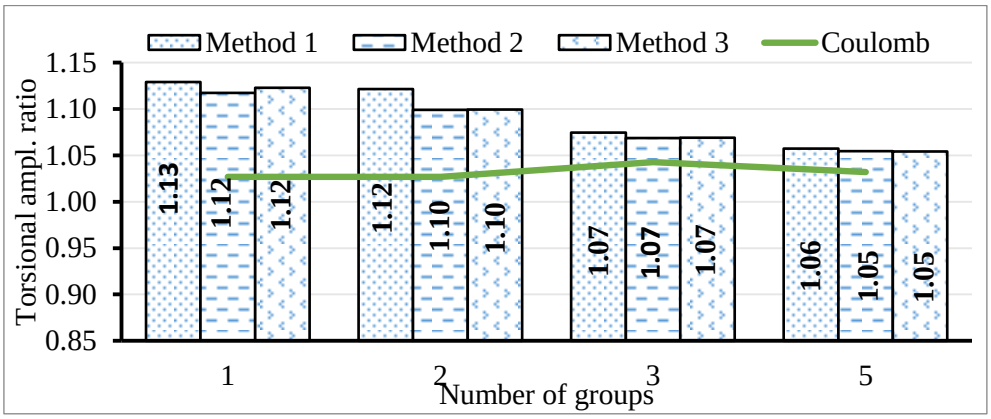

(b)

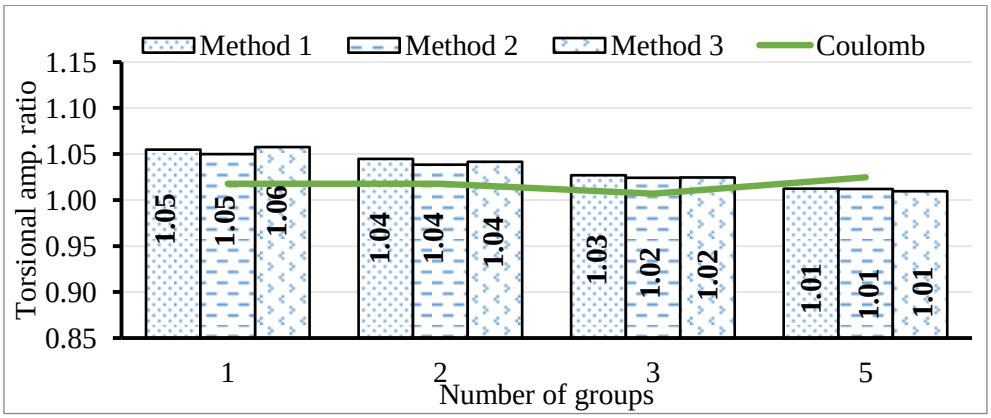

(c)

Figure 7-9. Torsional amplification ratio versus number of groups for three methods used for calculation of slider radius for (a) ‘Model A’, (b) ‘Model B’, (c) ‘Model C’.

7.3 Effect of isolation system static eccentricity

The effect of static eccentricity of isolation system is investigated. The results indicates that torsional amplification ratios increases as isolation system static eccentricity increases.

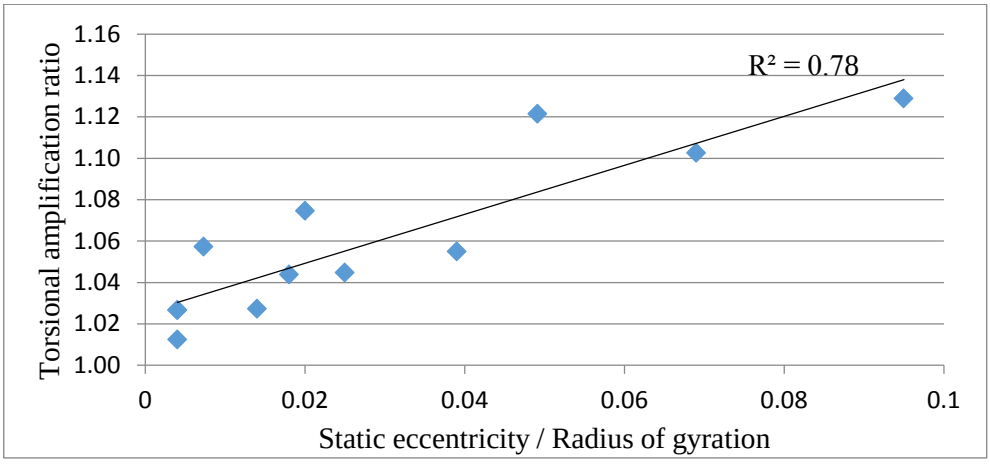

(a)

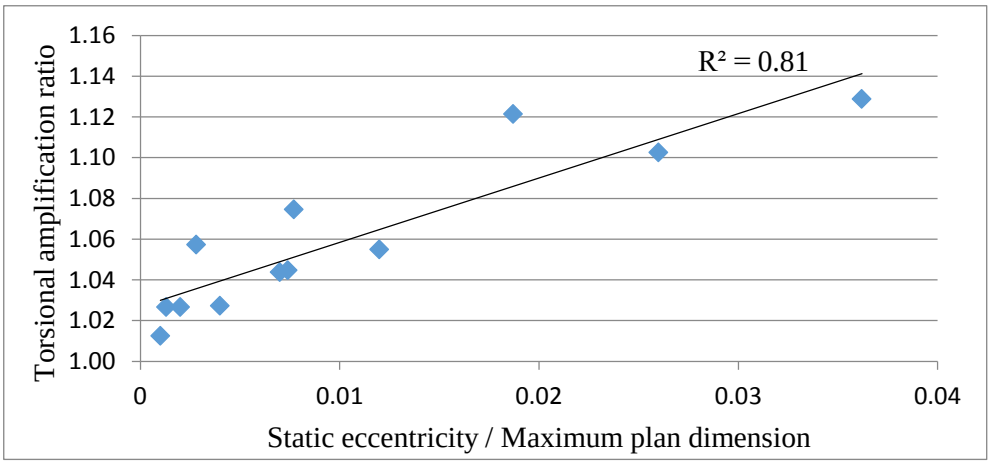

(b)

Figure 7-10. Torsional amplification ratio versus static eccentricity normalized by (a) radius of gyration, (b) maximum plan dimension.

CHAPTER 8

CONCLUSIONS

This study investigates the torsional response of structures that seismically isolated with Double Curved Surface Slider (DCSS) isolators, considering the effects of velocity, pressure and heating on friction inthe friction model.

The major conclusion that can be drawn from the study is that the effect of pressure and heating on the friction coefficient have a major influence on (1) displacement response of an individual isolator, (2) energy dissipation in isolator, and (3) torsion on the isolation system.

A friction model that ignores the heating effect may underestimate the peak displacements by about 10 to 15%, depending on location of the isolator, leading unconservative results. Such a friction model cannot capture degradation of the friction coefficient that results from heating during the course motion, and results in overestimation of friction coefficient. Similarly, the energy dissipation capacity of the isolators may be overestimated because of the overestimated friction coefficient. Essentially, the extent of the underestimation in displacement response can vary by isolator under consideration, as the effect of heating on friction depends on the liner material used in the sliding interface.

Experimental results conducted on double CSS isolators revealed that a friction model that ignores pressure-friction relationship may predict the friction coefficient significantly different than its actaul value.

It is found that the torsion on the isolation system may be significantly underestimated if the pressure and heating effects are not accounted for in the friction model.

The effect of vertical excitation is found to have minor effect on displacement response.

The importance of dynamic tests conducted on real size isolators under project-dependent velocity and load conditions for characterizing friction and force-displacement behavior of isolators under consideration has been emphasized by other studies. This study is not an exception to that observation. Although the underlying trends are similar, the friction-pressure and friction-heating relationships of the isolators used in this study are found different than those obtained by other studies.

A CSS-based isolation system has been considered in literature as an effective system against torsion since the center of rigidity of the system coincides with center of mass owing to fact that the lateral resisting force in a CSS isolator proportional to the axial load on it. This feature provides, unlike a traditional lateral force resisting system that consist of columns and shear walls, a constant shift in the center of rigidity of the system as the center of mass moves accidentally. It is found that the isolation system static eccentricity is small (less than 5% of maximum plan dimension), even for models whose isolators are not grouped based on axial loads. However, analyses performed herein revealed that significant torsion on the isolation system may still occurs, if the CSS isolators are not grouped and sized according to axial loads on it. It is also found that the torsional amplification increases as the isolation system static eccentricity increases.

It is observed that, in half of the analyses, the torsional amplification ratios is reduced by 1% when proposed ‘Method 2‘ or ‘Method 3’ are used instead of conventional ‘Method 1’, however, there is no clear trend of the effectiveness of these methods over the conventional method. ‘Method 2’ systematically yields a slider dimension slightly lower than that yielded by ‘Method 1’, and thus might be favoured due to economical considerations.

REFERENCES

Adzhemyan, A. (2017), "Experimental model for double concave sliding bearings", Master's thesis, Faculty of California State Polytechnic University

Al-Hussaini, T.M., Zayas, V.A., Constantinou, M.C., (1994), "Seismic Isolation of Multi-Story Frame Structures Using Spherical Sliding Isolation Systems"

Almazan, J.L., de la Llera, J.C., (2003) "Accidental torsion due to overturning in nominally symmetric structures isolated with the FPS", Earthquake Eng Struct Dynam, 32(6):919-48

American Association of State Highway and Transportation Officials (2010), "Guide Specifications for Seismic Isolation Design", Washington, D.C.

Anagnostopoulos, S. A., Kyrkos, M. T., Stathopoulos, K. G. (2015), "Earthquake induced torsion in buildings: Critical review and state of art", Earthquake and Structures, Vol 8, Issue 2, p: 305-377.

American Society of Civil Engineers (2016), "Minimum Design Loads and Associated Criteria for Buildings Other Structures", ASCE/SEI 7-16

Bowden, F.P., Tabor, D. (1964), "The friction and lubrication of solids – part II", Oxford University Press, London, Great Britain

Bao, Y., Becker, T. (2019), "Three-dimensional double friction pendulum bearing model including uplift and impact behavior: Formulation and numerical example", Engineering Structures, 199, 109579

BS EN, British Standart (2004), "Structural bearings Part 2: Sliding elements"

BS EN, British Standart (2004), "Structural bearings Part 7: Spherical and cylindrical PTFE bearings"

Buckle, I.G., Constantinou, M.C., Dicleli, M., Ghasemi, H. (2006), "Seismic Isolation of Highway Bridges", Report, MCEER-06-SP07, Multidisciplinary Center for Earthquake Engineering Research Center, Buffalo

Campbell, T. I., Pucchio, J.B., Roeder, C.W., Stanton, J.F. (1991), "Frictional Characteristics of PTFE Used in Slide Surfaces of Bridge Bearings", Proc. 3rd Word Congress on Joint Sealing and Bearing Systems for Concrete Structures, Toronto, Ontario, Canada, Vol. 2 of Preprints

CEN, European Committee for Standardization (2009), "EN 15129: Anti-Seismic Devices", Bruxelles, Belgium

Chang, K.C., Hwang, J.S., Lee, G.C. (1990), "Analytical model for sliding behavior of Teflon-stainless steel interfaces" Journal of Engineering Mechanics, 116(12), 2749-2763.

Clarke, C.S.J., Buchanan, R., Efthymiou, M., Shaw, C., (2005), "Structural Platform Solution for Seismic Arctic Environments—Sakhalin 2 Offshore Facilities", Offshore Technology Conference, Houston

Computers and Structures, (2016), "CSI Analysis Reference Manual"

Constantinou, M.C., Mokha, A., Reinhorn, A. (1990), "Teflon Bearings in Base Isolation 2: Modeling", J. Struct. En., 116(2):455-474

Constantinou, M.C., Tsopelas, P., Kasalanati, A., and Wolff, E.D. (1999), "Property modification factors for seismic isolation bearings", Report MCEER-99-0012, University at Buffalo, State University of New York, Buffalo, NY.

Constantinou, M.C., Whittaker, A.S., Kalpakidis, Y., Fenz, D.M., Warn, G.P. (2007), "Performance of seismic isolation hardware under service and seismic loading", Report MCEER-07-0012, University at Buffalo, State University of New York, Buffalo, NY.

Constantinou, M.C., Kalpakidis, I., Filiatrault, A., Lay, R.A.E. (2011), "LRFD-based analysis and design procedures for bridge bearings and seismic isolators" Report MCEER-11-0004, University at Buffalo, State University of New York, Buffalo, NY.

Çabuk, E., Akyüz, U., Yakut, A., Murota, N., Suzuki, S., Mori, T., Sütçü, F. (2020), "Performance comparison of high-damping rubber isolators and friction pendulum isolators with different modelling approaches", Report No:METU/EERC 2020-02, Earthquake Engineering Research Center, Middle East Technical University.

Dao, N.D., Ran, K.L., Sato, E., Sasaki, T. (2013), "Predicting the displacement of triple pendulum bearings in a full-scale shaking experiment using a three-dimensional element", Earthquake Engineering & Structural Dynamics, 42(11), 1677-1695.

Dolce, M., Cardone, D., Croatto, F. (2005) "Frictional Behavior of Steel-PTFE Interfaces for Seismic Isolation", Bulletin of Earthquake Engineering, 3:75-99.

Dicleli, M. (2020), personal communication.

Erdik, M. (2020), "Passive structural control applications in Turkey", https://www.youtube.com/watch?v=3p5yUDJzYBw (accessed 24 June 2021)

Feldstein, A., Goodman, R. (1973). "Numerical solution of ordinary and retarded differential equations with discontinuous derivatives", Numerische Mathematik, 21(1):1-13

Fenz, D.M, Constantinou, M.C. (2006) "Behaviour of the Double Concave Friction Pendulum Bearing", Earthquake Engineering and Structural Dynamics, ISSN: 00988847.

Fenz, D.M., Constantinou, M.C. (2008) “Development, Implementation and Verification of Dynamic Analysis Models for Multi-Spherical Sliding Bearings”, Report, MCEER-08-007, National Center for Earthquake Engineering Research, Buffalo

Fenz, D.M., Constantinou, M.C. (2008) “Mechanical Behavior of Multi-Spherical Sliding Bearings”, Report, MCEER-08-007, National Center for Earthquake Engineering Research, Buffalo

Gandelli, E. (2017), “Advanced tools for the design of sliding isolation systems for seismic-retrofitting of hospitals”, P.h.D. Dissertation, Department of Architecture, Built Environment and Construction Engineering

Gandelli, E., Penati, M., Quaglini, V., Lomiento, G., Miglio, E., Benzoni, G.M. (2018), “A novel OpenSees element for single curved surface sliding isolators”, Report, MOX-Report No. 13/2018, Politecnico di Milano

Gandelli, E., Penati, M., Quaglini, V., Lomiento, G., Miglio, E., Benzoni, G.M. (2019), “A novel OpenSees element for single curved surface sliding isolators”, Soil Dynamics and Earthquake Eng. Vol. 119: 433-453

Higashino, M., Hamaguchi, H., Minewaki, S., Aizawa, S. (2003). “Basic characteristics and durability of low-friction sliding bearings for base isolation” Earthquake Engineering and Engineering Seismology., Vol. 4, No 1

Huang, W.H. (2002) “Bi-directional Testing, Modeling, and System Response of Seismically Isolated Bridges”, P.h.D. Dissertation, Department of Civil and Enviromental Engineering, University of California, Berkeley

Kelly, J.M., (1997), “Earthquake-Resistant Design with Rubber”, 2nd ed, Springer-Verlag London.

Kumar, M., Whittaker, A.S., Constantinou, M.C. (2014), “Characterizing friction in sliding isolation bearings”, Earthquake Engineering and Structural Dynamics, Vol. 44(9):1409-1425

Kumar, M., Whittaker, A.S., Constantinou, M.C. (2015), “Seismic Isolation of Nuclear Power Plants using Sliding Bearings”, Report, MCEER-15-0006, Multidisciplinary Center for Earthquake Engineering Research Center, Buffalo

Kumar, M., (2017), “FPBearingPTV”, Open System for Earthquake Engineering Simulation (OpenSees), Pacific Earthquake Engineering Research Center (PEER), Berkely, USA. Available at: https://opensees.berkeley.edu/wiki/index.php/FPBearingPTV (accessed 24 June 2021)

Kumar, M., Whittaker, A., Constantinou, M. (2013) “Response predictions for Friction Pendulum Bearings considering the dependence of friction on axial pressure, temperature and velocity”, Transactions, SMiRT-22, San Francisco, California

Kumar, M. (2015), “Seismic isolation of nuclear power plants using sliding isolation bearings”, P.h.D. Dissertation, Department of Civil, Structural and Environmental Engineering, University at Buffalo

Mazza, F., Mazza, M. (2016), “Nonlinear seismic analysis of irregular r.c. framed buildings base isolated with friction pendulum system under near-fault excitations”, Soil Dynamics and Earthquake Engineering, 90: 299-312

Mazza, F., (2017), “Lateral-torsional response of base-isolated buildings with curved surface sliding system subjected to near-fault earthqaukes”, Mechanical Systems and Signal Processings, 92: 64-85

McKenna, F., Scott, M. H., and Fenves, G. L. (2010) “Nonlinear finite-element analysis software architecture using object composition.” Journal of Computing in Civil Engineering, 24(1):95-107.

McVitty, W.J., Constantinou, M.C. (2015), “Property modification factors for seismic isolators: design guidance for buildings”, Report MCEER-15-0005, University at Buffalo, State University of New York, Buffalo, NY.

Mokha, A., Constantinou, M.C., Reinhorn, A., (1990), “Teflon bearings in base isolation part 1: Testing.”, J. Struct. Engrg., ASCE, 116(2), 438-454

Mokha, A., Constantinou, M.C., Reinhorn, A.M. (1988), “Teflon bearings in Aseismic base isolation: Experimental studies and mathematical modeling.”, Report, NCEER-880038, National Center for Earthquake Eng. Res., State Univ. of New York, Buffalo

Mosqueda, G., Whittaker, A.S., Fenves, G.L., Mahin, S.A. (2004), “Experimental and Analytical Studies of the Friction Pendulum System for the Seismic Protection of Simple Bridges”, Report, California Department of Transportation Engineering Service Center, Sacramento

Nagarajaiah, S., Reinhorn, A.M., Constantinou, M.C. (1989), “Nonlinear Dynamic Analysis of Three Dimensional Base Isolated Structures(3D-BASIS)”, Technical Report, NCEER-89-0019, National Center for Earthquake Engineering Research, State University of New York, Buffalo

Nagarajaiah, S., Reinhorn, A.M., Constantinou, M.C. (1991), “3D-Basis: Nonlinear Dynamic Analysis of Three-Dimensional Base Isolated Structures: Part II, Technical Report, NCEER-91-0005, National Center for Earthquake Engineering Research, State University of New York, Buffalo

Ozdemir, G., (2010), “Response of isolated structures under bi-directional excitations of near-field ground motions”, P.h.D. Dissertation, Department of Civil Engineering, Middle East Technical University

Park, Y.J., Wen, Y.K., Ang, A.H-S. (1986), “Random Vibration of Hysteretic Systems under Bi-Directional Ground Motions”, Earthquake Engineering and Structural Dynamics, Vol.14

Pacific Earthquake Engineering Research Center, PEER Strong Motion Database. Available from: https://ngawest2.berkeley.edu. (accessed 24 June 2021)

Quaglini, V., Bocciarelli, M., Gandelli, E., Dubini, P. (2014) "Numerical Assessment of Frictional Heating in Sliding Bearings for Seismic Isolation", Journal of Earthquake Engineering, Vol 18(8): 1198-1216

Quaglini, V., Dubini, P., Poggi, C. (2012), "Experimental assessment of sliding materials for seismic isolation systems", Bulletin of Earthquake Engineering, Springer-Verlag, Berlin Heidelberg(D), Vol.10: 717-740

Quaglini, V., Gandelli, E., Dubini, P., (2018), "Influence of the static friction on the seismic response of a building isolated with slidin bearings", 16th European Conference on Earthquake Engineering, Thessaloniki

Sarlis, A.A.S., Constantinou, M.C., (2010), "Modeling Triple Friction Pendulum Isolators in Program Sap2000"

Sarno, L.D., De Risi, R., Paolacci, F., Marioni, A., Sartori, M., Taucer, F., Pegon, P. (2013), "Psuedo-Dynamic test of an old R.C. highway bridge with plain steel bars – part II: Investigation on the effectiveness of Yielding-based on FPS isolators", Second Conference on Smart Monitoring, Assessment and Rehabilitation of Civil Structures

Sarkistan, M., Lee, P., Hu, L., Doo, C., Zayas, V., Constantinou, M., Bachman, R. (2012), "Property Verification of Triple Pendulum Seismic Isolation Bearings", 20th Analysis & Computation Speciality Conference, ASCE

Scheller,J., Constantinou,M.C., "1999, Response History Analysis of Structures with Seismic Isolation and Energy Dissipation Systems: Verification Examples for Program Sap2000", MCEER-99-0002

Schellenberg, A. (2014), "Single Friction Pendulum Bearing Element", Open System for Earthquake Engineering Simulation (OpenSees), Pacific Earthquake Engineering Research Center (PEER), Berkely, USA. Available from https://opensees.berkeley.edu/wiki/index.php/FPBearingPTV (accessed 24 June 2021)

Simo, J.C., Hughes, T.J.R. (1998), "Computational Inelasticity", Springer New York

Soong, T.T., Constantinou, M.C. (1994), "Passive and Active Structural Vibration Control in Civil Engineering", Springer, New York

Su, L., Ahmadi, G., Tadjbakhsh, I.G. (1987) "Comparative Study of Base Isolation Systems", J. Engineering Mechanics, Vol. 115, No.9: 1976-1992

TBDY, 2018, Turkish Seismic Code for Buildings, Ministry of Public Works and Settlement Government of Republic of Turkey, Ankara, Turkey

Tsopelas, P.C., Roussis, P.C., Constantinou, M.C., Buchanan, R., Reinhorn, A.M., (2005), "3D-BASIS-ME-MB: Computer Program for Nonlinear Dynamic Analysis of Seismically Isolated Structures", Report MCEER-05-0009, National Center for Earthquake Engineering Research, Buffalo

Tyler, R.G. (1977), "Dynamic Tests on PTFE Sliding Layer under Earthquake Conditions", Bulletin of the New Zealand National Society for Earthquake Engineering, Vol. 10, No. 3, September, 129-138.

Ülker-Kaustell, M. (2017), "Dynamic behavior of pot bearings", Report, Report 168, Royal Institute of Technology(KTH), Stockholm

Yang, T., Calvi, P.M., Wiebe, W. (2020), "Numerical implementation of variable friction sliding base isolators and preliminary experimental results", Earthquake Spectra, Vol. 36(2), 767-787

Wen, Y.K. (1976), "Method for Random Vibration of Hysteretic Systems", Journal of the Engineering Mechanics Division, ASCE, Vol. 102, No. EM2.

Wilson, E.L., (2002), "Three-Dimensional Static and Dynamic Analysis of Structures A Physical Approach With Emphasis on Earthquake Engineering", 3ed.

Wolff, E.D., Ipek, C., Constantinou, M.C., Morillas, L. (2014), "Torsional response of seismically isolated structures revisited", Eng. Structures, 59: 462-468.

Zayas, V., Low, S.S., Mahin, S.A. (1987), "The FPS earthquake resisting system, experimental report" Report No. UCB/EERC-87/01, Earthquake Engineering Research Center, Univ. of California, Berkeley, Calif.